

# Analysis of Tropical Cyclones Using Microwave Satellite Imagery

**Jun'ichi ASANO**

Meteorological College, Japan Meteorological Agency (JMA)  
7-4-81, Asahi-cho, Kashiwa, Chiba, 277-0852 Japan

**Shuuji NISHIMURA<sup>i</sup>, Koji KATO<sup>ii</sup>, Kouki MOURI<sup>iii</sup>, Sadao SAITOH<sup>iv</sup>,  
Shiro YOSHIDA<sup>iii</sup>, Takeshi ENDO<sup>v</sup>, Kohei OOTUBO<sup>v</sup>, Akihiro SHIMIZU<sup>iii</sup>,  
Ryo OYAMA<sup>ii</sup>**

## Abstract

The Meteorological Satellite Center of the Japan Meteorological Agency has estimated center positions and intensities of tropical cyclones by the *Dvorak method*, which uses infrared and visible imagery from the *MTSAT-1R* geostationary meteorological satellite. While the Dvorak method is the most popular technique for analyzing tropical cyclones through infrared and visible imagery, it is not good at estimating the center positions of tropical cyclones that are covered by upper cirrus cloud and do not have a clear eye in their developing stage, especially during periods when visible imagery is not available.

To combat this difficulty, we used microwave imagery from the *AMSR-E* system on board the *Aqua* earth-observing satellite to analyze the inner structures of tropical cyclones, which cannot be seen in infrared or visible imagery. We also developed a method to estimate center positions of tropical cyclones using this microwave imagery analysis. Verification using the tropical cyclones from 2003 to 2005 showed that the accuracy of center positions estimated by microwave imagery was almost the same as that obtained by radar observation. As a result, our method was proven to be an effective means of improving the accuracy of center positions estimated by the Dvorak method.

---

<sup>i</sup> National Typhoon Center, Forecast Division, Forecast Department, JMA

<sup>ii</sup> System Engineering Division, Data Processing Department, Meteorological Satellite Center, JMA

<sup>iii</sup> Analysis Division, Data Processing Department, Meteorological Satellite Center, JMA

<sup>iv</sup> Earth Observation Research Center, Japan Aerospace Exploration Agency

<sup>v</sup> Satellite Control Division, Data Processing Department, Meteorological Satellite Center, JMA

## 1. Principle of Observation with Microwave Imagery

A microwave radiation usually refers to an electromagnetic wave with a frequency of 3 to 30 GHz or a wavelength of 10 to 1 cm (Table 1-1). The frequency range of microwaves for actual observation by satellites includes frequencies that are relatively higher than the range defined in the table, and electromagnetic waves with those frequencies are also called microwaves here for the sake of convenience. Generally, microwave observation equipments are classified according to the observation method and purpose; however, it is generally called a microwave sensor here.

Satellite observation using microwaves requires a frequency range that is significantly lower (or with a longer wavelength range) than that for infrared sensors with geostationary meteorological satellites (10- $\mu$ m range, which is called the infrared range hereinafter) or for visible sensor (0.6  $\mu$ m range). Therefore, with limited influence of cloud particles, satellite observation can tell atmospheric conditions under the cloud top. This advantage of microwave sensors that has not been achieved by infrared or a visible sensor presents an absolutely new viewpoint for the analysis of weather phenomena. On the other hand, information that has been accumulated through analysis using infrared and visible imagery may not be applied to analysis with microwaves directly. Therefore, it is important to know the characteristics of the new method with microwaves.

Chapter 1.1 describes the characteristics of microwaves necessary for the analysis of weather phenomena, such as tropical disturbance.

Chapter 1.2 describes classified typical satellites equipped with microwave sensors, and their observation methods.

Chapter 1.3 indicates key points necessary for actual analysis of weather phenomena using imagery produced from observation data obtained with microwave sensors. The same chapter also describes characteristics and provides notes for the wavelength range used for analysis.

For abbreviations in this document, see “Appendix 2 Abbreviations.”

### 1.1 Characteristics of the Microwave Range

Table 1-1 Frequencies, wavelengths, and names of electromagnetic waves

Frequency (Hz)	Wavelength (m)	Name
$3 \times 10^{22}$	$10^{-14}$	Gamma ray
$3 \times 10^{21}$	$10^{-13}$	
$3 \times 10^{20}$	$10^{-12}$	
$3 \times 10^{19}$	$10^{-11}$	X ray
$3 \times 10^{18}$	$10^{-10}$ (1 Å)	
$3 \times 10^{17}$	$10^{-9}$ (1 nm)	Ultraviolet ray
$3 \times 10^{16}$	$10^{-8}$	
$3 \times 10^{15}$	$10^{-7}$	Visible light
$3 \times 10^{14}$	$10^{-6}$ (1 $\mu$ m)	
$3 \times 10^{13}$	$10^{-5}$	Infrared ray
$3 \times 10^{12}$ (3 THz)	$10^{-4}$	
$3 \times 10^{11}$	$10^{-3}$	Submillimeter wave
$3 \times 10^{10}$	$10^{-2}$ (1 mm)	
$3 \times 10^9$ (3 GHz)	$10^{-1}$ (1 cm)	<b>Microwave</b>
$3 \times 10^8$	1	Ultrashort wave
$3 \times 10^7$	$10^1$	Short wave
$3 \times 10^6$ (3 MHz)	$10^2$	
$3 \times 10^5$	$10^3$ (1 km)	Medium wave
$3 \times 10^4$	$10^4$	
$3 \times 10^3$ (3 kHz)	$10^5$	Long wave
$3 \times 10^2$	$10^6$	Ultralong wave

The microwave range is in a significantly lower-frequency range (or longer-wavelength range) than the visible or infrared ranges (Table 1-1). As with the case of the infrared range, the microwave range acts as the atmospheric window, and is suitable for satellite observation with limited influence of the atmosphere (Figure 1-1). However, the energy within microwave range is significantly small; the scale is a ten-billionth of that of the infrared range. Therefore, satellites equipped with microwave sensors orbit at the altitude (400 to 900 km) significantly lower than geostationary orbit (about 36000 km) to achieve gain (see Chapter 1.2).

As shown in Figure 1-2, influences by the earth's surface conditions and atmosphere, and various types of particles in the atmosphere, on a microwave depend on its wavelength. This means that it is necessary to select a suitable wavelength to observe a target object. The atmosphere is nearly transparent to a wavelength of 10 GHz or lower. The sea surface temperature is sensitive to the same-wavelength range. The higher the wavelength, the lower the response to the surface temperature. On the other hand, the higher the wavelength, the higher the response to water clouds. Water vapor affects the response of the entire microwave range.

The following pages describe the general characteristics of microwaves. For characteristics of microwaves not mentioned in this chapter or details on theoretical background, see, for example, Hayasaka (ed., 1996) mentioned in the References.

### 1.1.1 Atmospheric Influences

Satellite observation of the earth, including that with microwaves, is performed by receiving radiation energy from the earth by satellite sensors, which measure physical quantities with the dimension of energy. Radiation energy emitted from the earth is affected by the air, cloud particles, and raindrops on its way to a satellite sensor. According to usage, energy detected by such sensors is

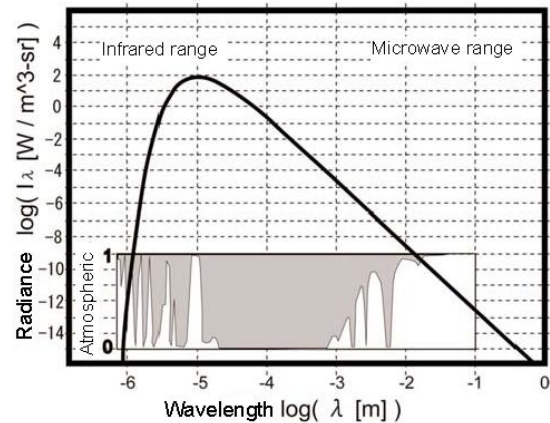


Figure 1-1 Earth radiation spectra and atmospheric transmittance

The radiance of earth radiation is calculated based on the model of a black body of 290 K. For atmospheric transmittance, the height of white spaces corresponds to the strength of a transmittance.

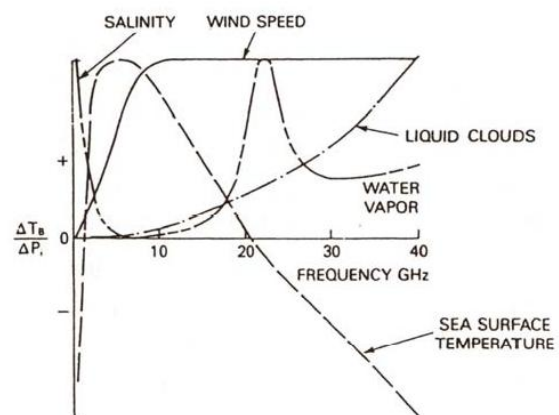


Figure 1-2 Rates of changes in radiation temperature of microwave radiation with respect to various changes in objects to be observed with microwave remote sensing (NASA, 1987)

converted into radiance temperature, or effects of the air on the energy are estimated to retrieve physical quantities.

The microwave range generally has high atmospheric transmittances, so it is easy for microwave radiation from the earth's surface to reach a satellite sensor. This means that information about the surface is easily obtainable.

Microwave radiation with a suitable-frequency transmits clouds, which is nearly opaque to the infrared region, so that conditions inside clouds can be clear. For clouds, satellite observation can tell not only the top using the infrared region, but also the inner structure using the microwave range.

To understand the observation mechanism for the inner structure of clouds, it is necessary to know the influences by cloud particles, raindrops, and snow particles on microwaves. Particles of water and ice absorb, emit, and scatter microwave radiation. The degree of influences is greatly different between water and ice particles, and depends greatly on the frequency of an incoming wave.

Generally, water clouds have a high microwave absorptivity, and therefore, a high emissivity. This feature and the low emissivity of the sea surface are reasons for the higher radiation temperature of water clouds than that of the sea surface.

Ice particles such as snow and hail are good scattering bodies of microwaves. This property becomes more significant with an increase in microwave frequency. A high scattering property reduces the volume of radiation that reaches a satellite sensor, leading to lowered radiation temperature. Therefore, well-developed convection clouds in which many ice particles are present above the melting layer are recognized as a region of low radiation temperature, especially in a high-frequency band of the microwave range.

The information given in this section is presented in schematic form as shown in Figure 1-3. Figure 1-3(A) is a schematic diagram of the 89-GHz band.

In the case of A-1, almost the entire radiation emitted by the sea surface is directly observed by a satellite sensor because the influences by high-altitude clouds consisting of ice crystals on microwave radiation are negligible. Water clouds (A-2) absorb and reemit most parts of microwaves emitted by the sea surface. A satellite observes the sum of radiation from the sea surface and water clouds, and the emissivity of water clouds is nearly 1, so the brightness temperature of water clouds is higher than that of the sea surface. In well-developed convection clouds (A-3), radiation is affected by scattering particles such as snow and hail, so the amount of radiation that reaches a satellite is significantly reduced. Therefore, the brightness temperature is also greatly reduced. Figure 1-3 (B) is a schematic diagram of the 36-GHz band. In the case of B-1, a microwave in this band is transmitted through high-altitude clouds in the same way as that in the 89-GHz band. However, the emissivity of the sea surface for the band is significantly low, so its brightness temperature is significantly low. Because microwave radiation in the 36-GHz band is largely reemitted by water clouds (B-2), the brightness temperature of water clouds is higher than that of the sea surface. In well-developed convection clouds (B-3), microwave radiation in the 36-GHz band is scattered, but is not as scattered as that in the 89-GHz band, so the reduction in the brightness temperature is small.

The frequency range of the microwave shown in Figure 1-3 is considered appropriate for tropical disturbance analysis and is described in detail in Chapter 1.3.

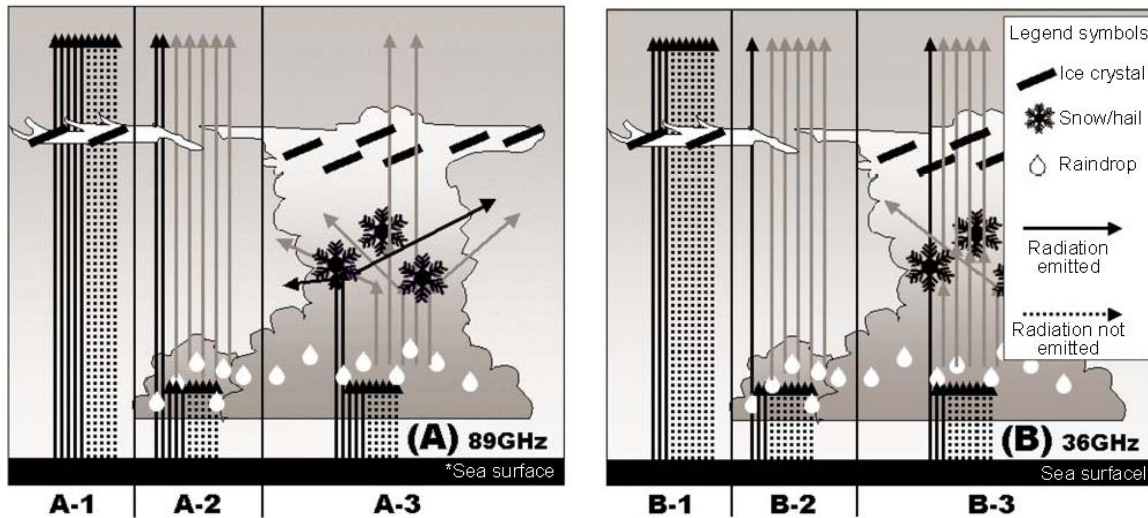


Figure 1-3 Schematic diagram of atmospheric influences on microwave channels

(A) Schematic diagram of 89-GHz band: A-1: Clear weather or clouds only at high altitude; A-2: Water clouds; and A-3: Well-developed convection clouds

(B) Schematic diagram of 36-GHz band: B-1: Clear weather or clouds only at high altitude; B-2: Water clouds; and B-3: Well-developed convection clouds

As the sea emissivity for microwaves is lower than 1, the solid-line arrows indicate radiation actually emitted, and the dotted-line arrows indicate radiation supposed to be emitted if the emissivity is 1. In this diagram, the amount of energy is proportional to the number of arrows. The diagram is prepared supposing no effects of water vapor on the assumption that the sea temperature would be the same. Because the diagram is prepared schematically for easy understanding, the numbers of the arrows in the diagram do not always correspond to actual measurements.

### 1.1.2 Relationship between the frequency range and horizontal resolution

Wavelengths of the microwave range are in the range of 1 centimeter to 10 centimeters. Because the energy of an electromagnetic wave increases in reverse proportion to its wavelength, the horizontal resolution of the shortest-wavelength band (highest frequency) is approximately 10 times higher than that of the longest-wavelength band (lowest frequency) when a wave is observed at the same altitude by an antenna with the same diameter.

Horizontal resolutions of microwave sensors are listed according to their frequencies in Appendix 1 Satellites and Sensors, which shows that the higher the frequency, the higher the resolution.

Such differences in resolution by frequency can be an important factor when you discuss the accuracy of the location of a typhoon eye, for example.

### 1.1.3 Emissivity of the earth's surface

Generally, an object emits an electromagnetic wave with reference to its temperature. A black body has an emission rate of 1. This means that the radiance temperature calculated using the strength of an electromagnetic wave emitted from the body is equivalent to the temperature of the body itself.

In the infrared region, for example, ground surface, which can be considered a black body, has an emissivity of approximately 1. This suggests that the radiance temperature of unclouded areas in the infrared range is considered to be the temperature of the ground surface.

In the microwave range, on the other hand, the ground surface cannot be considered a black body. Depending on the frequency, the emissivity in the microwave range is basically lower than 1 (Figure 1-4). This indicates that the radiance temperature of the ground observed with a microwave is lower than the actual temperature of the ground surface. This decrease is significant especially on the sea surface, where the emissivity is much lower than 1. This influence is further pronounced on a low-frequency band of the microwave range, with which the radiance temperature of the sea surface is found to be extremely low. Great differences in radiance temperature are observed between the sea surface (extremely low radiance temperature), and water clouds (relatively high radiance temperature achieved by radiation from the clouds, which have an emissivity of approximately 1). Therefore, water clouds appear as regions of high radiance temperature, and can be easily distinguished from the sea surface.

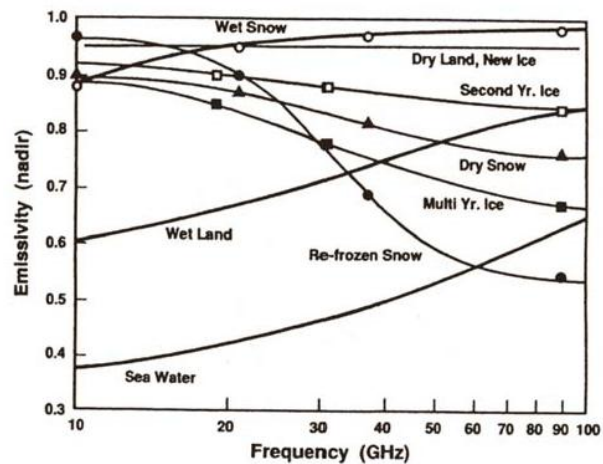


Figure 1-4 Emissivity of different ground surfaces for the microwave range (Grody, 1993)

### 1.1.4 Polarization (vertical and horizontal)

A microwave is a type of electromagnetic wave and is a transversal wave with its electric and magnetic fields oscillating at right angles to each other (Figure 1-5). An electromagnetic wave whose electric field oscillates at a right angle to the reflection surface (ground surface) is called the vertical polarization. An electromagnetic wave whose electric field oscillates in a plane horizontal to the ground surface is called the horizontal polarization.

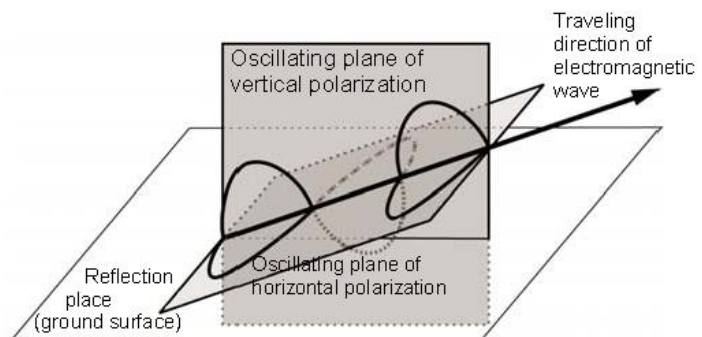


Figure 1-5 Schematic diagram of vertical and horizontal polarizations

Among microwave sensors, many types of imagers measure different polarizations for each frequency.

Intensities of different components are measured because different components have different properties, which allows estimation of atmospheric influences, especially scattering influences.

On a plane horizontally homogeneous and smooth, the emissivity of a vertical polarization is higher than that of a horizontal polarization because of Fresnel's law and Kirchhoff's law. This means that when a calm sea surface is observed with a microwave, the brightness temperature of a vertical polarization is higher than that of a horizontal polarization. The difference in brightness temperature between these two waves depends on the frequency of a microwave, but the brightness temperature of a vertical wave is always higher than that of a horizontal wave.

If vertical and horizontal polarizations are affected by scattering particles on their way to a satellite sensor, scattering changes the oscillating direction of the electric field of a wave in various directions. Therefore, scattering effects on a microwave decreases the difference in brightness temperatures between its vertical and horizontal polarizations. Using this property, it is possible to distinguish between the sea surface and well-developed convection clouds using a measurement of radiance temperature for the region.

## **1.2 Types of microwave sensors and satellites**

### **1.2.1 Orbits of satellites equipped with a microwave sensors**

Satellites equipped with a microwave sensor orbit at an altitude of approximately 400 to 900 kilometers. They take 90 to 100 minutes to make an orbit of the earth. Unlike geostationary meteorological satellites, which are in stationary orbit of the earth and take images of the same area, many satellites equipped with a microwave sensor make an orbit of the earth in a short cycle, and observe strip-shaped areas several-thousands-kilometer wide, as described on the next section.

Because this observation method limits the area that can be observed while a satellite make an orbit, in most cases, a slight change is made to a satellite's orbit when it has made an orbit so that images taken in different orbits cover almost the entire earth. Many satellites orbit over both poles of the earth. Such orbits are called polar orbits, and satellites that take polar orbits are called polar orbiter. Typical polar orbiters equipped with a microwave sensor include the Aqua satellite, DMSP satellite series, and NOAA satellite series. These satellites orbit the earth while keeping the angle between their orbital planes and orientations toward the sun the same. Such orbits are called sun-synchronous orbits. Its advantage is that an area can be observed twice a day at the same local times. This reduces the influences of changes in sunlight.

An orbit in which a satellite returns to its starting point within 24 hours after it has made some orbits is called a recurrent orbit. An orbit in which a satellite returns to its starting point after more than 24 hours and within several days is called a sub-recurrent orbit. Most polar orbiters take the sub-recurrent orbit because the coverage of satellites is wide and they return to the starting point regularly.

In summary, the above-mentioned orbit of polar orbiters can be called the sun-synchronous

sub-recurrent orbit. This orbit possesses many advantages: a satellite in this orbit returns to the starting point in a cycle of several days while it observes the same area at the same local time under the same conditions where a satellite keeps its positional relationship with the sun the same.

On the other hand, the TRMM satellite does not take the polar orbit. The angle between the satellite's orbit plane and the equatorial plane is 35 degrees. It observes the area ranging between 35 degrees north and 35 degrees south of the equator. This satellite is not sun synchronous because it observes day changes in the rainfall in the tropical region at different local time.

### **1.2.2 Passive and Active Sensors**

Satellite observation with a microwave is roughly classified into two according to the sensor types: a passive sensor or an active sensor.

A passive sensor receives microwave radiation that is emitted naturally from the earth. This is the same observation mechanism as for infrared imagers for geostationary meteorological satellites. As mentioned in the first part of this section, the energy of the microwave range by earth radiation is very small. Generally, the energy received by an antenna is proportional to its diameter, and inversely proportional to the distance to the observation object. Therefore, in order to achieve gain, satellites are orbited at a low altitude or equipped with a large antenna. However, despite these efforts, the temperature resolution of passive sensors is still lower than that of infrared imagers.

Typical passive sensors for the microwave range are: AMSR-E, loaded on the Aqua satellite; SSM/I, loaded on the DMSP satellite series; TMI, loaded on the TRMM satellite; and AMSU-A, AMSU-B, and MHS, loaded on the NOAA satellite series. Data obtained with these passive sensors are used to analyze weather phenomena using their brightness temperatures. This is described in detail later.

An active sensor itself emits a microwave like a radar, and observes a wave reflected by an object. For example, SeaWinds, loaded on the QuikSCAT satellite, measures the direction and speed of winds over the sea by detecting the scattering state of a microwave, which is scattered in a different way according to the sea surface state. The TRMM satellite has a 14-GHz precipitation radar to observe precipitation. The CloudSat satellite has a 94-GHz radar to detect the three-dimensional structure of clouds. As represented by these examples, an active sensor is used to obtain specific physical products, such as wind or rain.

### **1.2.3 Imager and sounder**

As with an infrared sensor, a microwave passive sensor is classified into an imager and a sounder.

An imager is observational equipment to covert data into images with a relatively high horizontal resolution. Typical imagers include: AMSR-E, loaded on the Aqua satellite; SSM/I, loaded



on the DMSP satellite series; and TMI, loaded on the TRMM satellite. For each observation frequency, these imagers observe its vertical and horizontal polarizations, which are described in Chapter 1.1.4, and convert obtained data into images.

A sounder is equipment to observe different frequencies in order to obtain vertical profiles of physical quantities for a purpose, such as air temperature distribution and water vapor distribution. A sounder is configured to observe many frequencies at and around a specific absorption line according to a physical quantity to be obtained. For its high wavelength resolution, a sounder trades off horizontal resolution. Generally, a sounder has a lower horizontal resolution than an imager. Typical sounders of microwave sensors are AMSU-A, AMSU-B, and MHS, loaded on the NOAA satellite series. AMSU-A is designed to obtain temperature profiles, while AMSU-B and MHS are designed to obtain vertical water vapor profiles.

Unlike an imager, a sounder is designed mainly to obtain vertical profiles of physical quantities, so it observes either a vertical polarization or a horizontal polarization.

To analyze a meteorological phenomenon using its graphic information, an imager is more suitable. It is possible to use a sounder using a selected frequency in the same way as an imager, but a lower horizontal resolution than that of an imager is produced. A sounder has a disadvantage in that polarization information is unavailable. Observation with a microwave sensor is performed with insufficient frequency, so the use of microwave data obtained with a sounder is of value.

#### 1.2.4 How to Scan with Microwave sensors

There are two main modes of antenna scanning to observe the earth with a microwave sensor: the conical scanning, and the cross-track scanning.

Conical scanning is a mode of scanning by antenna rotation on the base of a satellite as shown in Figure 1-6. This mode is named “conical scanning” because an antenna at a constant angle with respect to the vertical direction moves in a conical form while scanning the ground. Because conical scanning observation keeps the angle that the antenna forms with ground the same, the size of FOV (Field Of View: the area that a sensor can view at one time) is constant during observation, so that the angular characteristics of radiation are maintained. Therefore, the conical scan mode is used in many types of microwave imagers that observe both the horizontal and vertical polarizations, including all of the imagers mentioned in the previous section. Because of the constant antenna angle, the swath

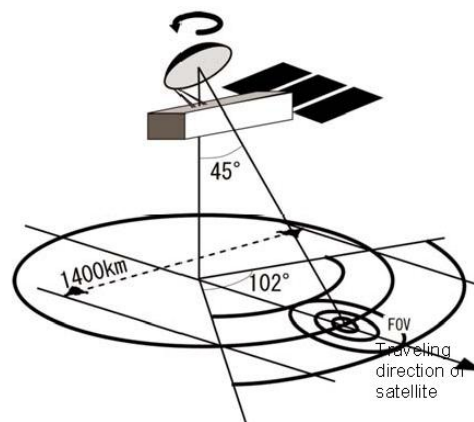


Figure 1-6 Schematic diagram of conical scanning  
The concept of conical scanning is represented graphically, using SSM/I as an example.

width is lower than that for the track scanning mode. Figure 1-6 shows an example of SSM/I. Among nested FOVs, an FOV that is closer to the center of the nest is dedicated to observation of a higher frequency, and a higher resolution is produced by a higher frequency.

Cross-track scanning is a mode of scanning by antenna movement along the direction perpendicular to the traveling direction of a satellite. Therefore, the FOV is minimal at the point at which the satellite observes directly below it, and is greater at a position that is further from the minimal position. Because the angle that the antenna forms with the ground is changed, angle characteristics are not maintained. On the other hand, the swath width of the cross-track scanning can be greater than that of the conical scanning. Most sounders adopt cross-track scanning. The cross-track scanning mode is used in all sounders mentioned in the previous section. As shown in Figure 1-7, prepared using AMSU-A and -B as examples, the FOV of AMSU-B, dedicated to observation with a higher frequency, is inside the FOV of AMSU-A.

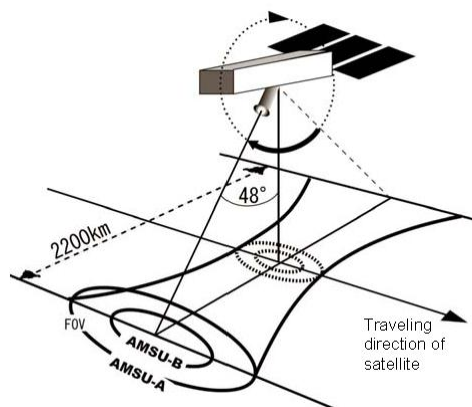


Figure 1-7 Schematic diagram of cross-track scanning. The concept of cross-track scanning is presented schematically, using AMSU-A and -B as examples.

### 1.3 Analysis with microwave imagery

This section describes important things for analyzing meteorological phenomena based on the properties of microwaves and characteristics of the observation method.

As shown in “Appendix 1 Satellites and Sensors,” a microwave sensor uses many frequencies for observation. However, not all data converted into graphic data are suitable for the analysis of meteorological phenomena. Therefore, it is necessary to select frequencies suitable for the operational application of tropical disturbance analysis (Kato et al., 2004) performed at the Meteorological Satellite Center.

This section describes an analysis with frequencies used in surveys described in Chapter 2 or later. Frequency bands are named from the observation frequencies of AMSR-E. Slightly different frequencies are used in other sensors for observation (e.g., 89 GHz is used for AMSR-E, while 85.5 GHz is used for SSM/I). Observation frequencies are different according to the sensor, but are selected essentially within the frequency band that has the same characteristics. Differences in observation frequencies selected in this way have few effects on the analyses described later, so the same name is given to the selected observation frequencies for the sake of convenience.

The 89-GHz and 36-GHz bands are selected to analyze tropical cyclones. In next section and later, their characteristics are described based mainly on advantages and disadvantages for analysis.

However, interpretation of microwave images is under development, and many aspects remain insufficiently revealed. It should be noted that with preceding studies, such as those by Randall et al. (1992 and 1993), as a guide, characteristics of selected frequencies are extracted and described based on frequencies and actual radiation temperature distributions that have been illustrated.

Points to consider for tropical disturbance analysis are mainly provided after description of the two selected frequency bands

### **1.3.1 Characteristics of the 89-GHz band**

The 89-GHz band is a relatively high-frequency band of the microwave range with a relatively high horizontal resolution (about 6 kilometers for AMSR-E). The main characteristic of the band is that it is greatly scattered by ice particles such as snow or hail. Therefore, well-developed convection clouds are found to be areas of extremely low radiance temperature (c1 and c2 areas in Figure 1-9).

Based on this property, especially in tropical disturbance analysis, the area of the strongest convection stands out in a well-developed convection cloud such as the Cb band, and is easily identifiable.

Other characteristics can be explained by the previously described properties of the microwave.

As compared with the land (with an emissivity of about 1), the sea surface (with an emissivity of lower than 1) is found to be a region of lower radiation temperature (around b1 and b2 in Figure 1-9). Because of absorption and scattering by water cloud particles or raindrops, water clouds below the melting layer are found to be a region of relatively higher radiation temperature than that of the sea surface (around e1 and e2 in Figure 1-9).

Using these characteristics, the main analytical work using these frequency bands is tracking of areas of low radiation temperature of well-developed convection clouds. Generally, it is useful to limit the object to be observed with a microwave to the sea surface. However, because well-developed convection clouds stand in sharp contrast to the land, which appears as a region of high radiation temperature, it is possible to keep track of such clouds over the land.

It should be noted that well-developed convection clouds and a sea surface with low surface temperature may be confused because their radiation temperature is found to be similar. For example, a typhoon over a sea area with low surface temperature should be carefully analyzed.

To avoid this kind of confusion, a good method is comparison of radiation temperature between the vertical and horizontal polarizations. If a microwave is sufficiently scattered in a convection cloud, the radiation temperature of the vertical polarization will be nearly the same as that of the horizontal polarization. Therefore, well-developed convection clouds are distinguishable from the sea surface, which makes a great difference in radiation temperature between the vertical and horizontal polarizations of a microwave.

An example of this is shown in Figure 1-8. In Figure 1-8 (A) of infrared imagery, no clouds are observed over the Yellow Sea or sea area in the southern part of Okinawa. The radiation temperature

is about 283 K and 293 K, respectively, which makes a difference of about 10 K. Looking at the microwave imagery of Figure 1-8 (B) and (C), the brightness temperature of the Yellow Sea is found to be much lower than that of the sea area in the southern part of Okinawa, and almost the same as that of the convection cloud accompanied by Typhoon No. 200601 around the Philippines. These figures clearly show some change in radiation temperature between the vertical and horizontal polarizations in the region of low brightness temperature caused by the active convection cloud accompanying the typhoon. And in the Yellow Sea, the brightness temperature of the horizontal polarization is lower than that of the vertical polarization, which makes a great difference between them.

Another effective discrimination method is the use of polarized corrected temperature (PCT) (Spencer et al. 1989). Using calculated PCT values, effects of polarization by the sea surface or water drops can be eliminated to extract a decrease in radiation temperature by scattering, so that convection clouds are easily identifiable. The Meteorological Satellite Center provides calculated results of different radiation temperatures, including PCTs, in real time, but this service is in the trial-and-error stage.

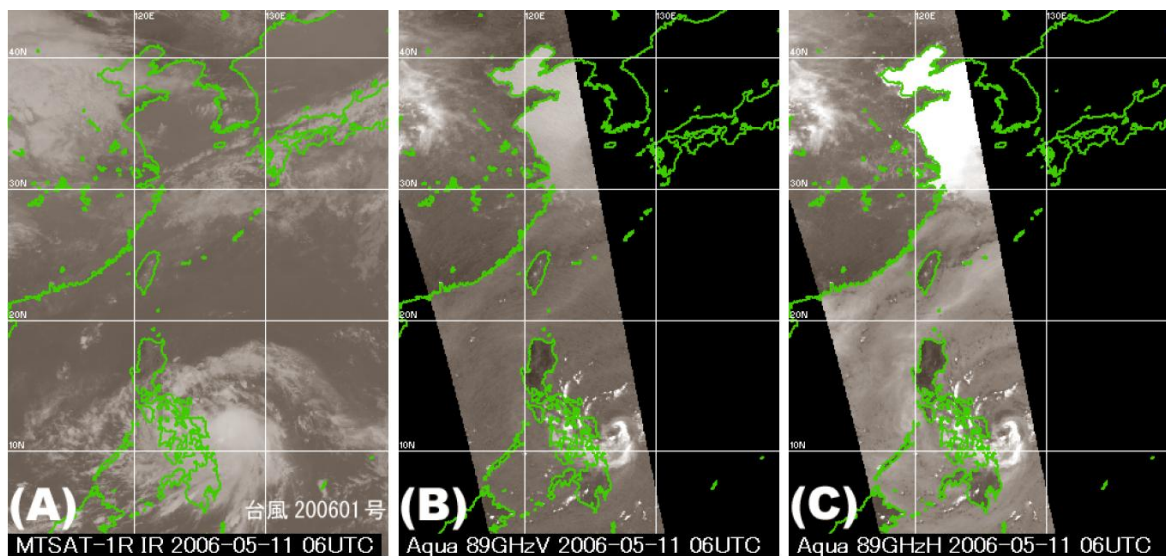


Figure 1-8 Images of vertical and horizontal polarizations of the 89-GHz band (06 UTC, May 11, 2006)  
 (A) Infrared image, (B) Vertical polarization, and (C) Horizontal polarization  
 In each image, a darker region (black) indicates a region of higher brightness temperature, and a lighter region (white) indicates a region of lower brightness temperature.

### 1.3.2 Characteristics of 36 GHz

The 36-GHz band is a middle-frequency band of the microwave range with a lower horizontal resolution than that of the 89-GHz band (about 14 kilometers for AMSR-E). The main characteristic of the band is that the sea surface is found to be a region of low radiation temperature, and microwaves are strongly affected by water clouds. Because absorption and emission by precipitation

particles and cloud particles affect microwaves in the 36-GHz band more strongly than in other frequency bands, water clouds are found to be a region of high brightness temperature (f3 and f4 areas in Figure 1-9). The sea surface is found to be a region of extremely low radiation temperature because of the low emission rate (around b3 and b4 in Figure 1-9).

These characteristics allow identification of water clouds over the sea as a region of high brightness temperature with high contrast, so detection of water clouds over the sea is the main analytical work using the 36-GHz band. However, observation of water clouds over the land is impossible because the emissivity of the land is high and the radiation temperature is high.

It should be noted that in some cases, effects of scattering by ice particles such as snow or hail on the 36-GHz band are not negligible. A decrease in the radiation temperature of this band is not negligible for extremely well-developed convection clouds such as a typhoon. In this case, it is necessary to distinguish whether a region of low radiation temperature comes from the sea surface or a convection cloud. To distinguish these differences, it is effective to use polarization data, as described in the section of the 89-GHz band (see Chapter 1.3.3). A region with a great difference in radiation temperature between the vertical and horizontal polarizations suggests the sea surface and a region with a small difference suggests a well-developed convection cloud.

### **1.3.3 Microwave imagery comparison**

Using Figure 1-9, characteristics of the 89-GHz and 36-GHz bands are explained through comparison of graphical representation between them. In this section, Figures 1-9 (A) to (E) are abbreviated to (A) to (E), respectively.

Two cloud masses clearly shown in the infrared image (A) indicate typhoons: the one over the sea area in the southern part of the major island of Japan is numbered 200607, and the other at a latitude of approximately 20 degrees north is numbered 200608. Infrared image (A) shows a case example in which analyses of the eyes of Typhoon Nos. 200607 and 200608 are difficult.

In microwave images (B) to (E), the land surface (e.g., a1 to a4 of each image) exhibits the highest radiation temperature, and appears as dark areas. The sea surface (e.g., b1 to b4 of each image) appears as dark areas (b1 and b2) with the 89-GHz band having a relatively high emissivity, and as light areas (b3 and b4) with the 36-GHz band having a low emissivity. On the sea surface in each frequency band, vertical polarization (b1 and b3) is higher in brightness temperature than horizontal polarization (b2 and b4), and the sea surface appears as dark areas. The sea surface exhibits a great difference in radiation temperature between the horizontal and vertical polarizations.

In images (B) and (C) of the 89-GHz band, areas (e.g., c1 and c2) of active convection clouds affected by scattering by ice particles over the melting layer are extremely low in radiation temperature, and appear as glistening white. In Typhoon No. 200608, an area of high radiation temperature at a latitude of 20 degrees north suggests its eye (d1 and d2). Concerning Typhoon No. 200607, water clouds (e1 and e2) appear as relatively dark areas that are warmer than the sea surface



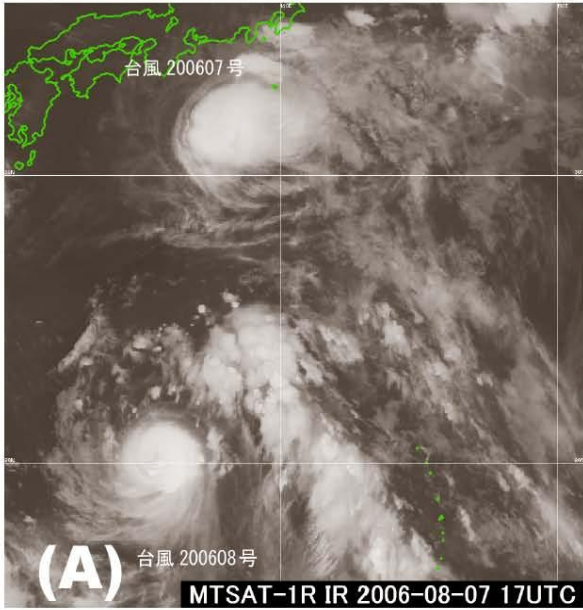
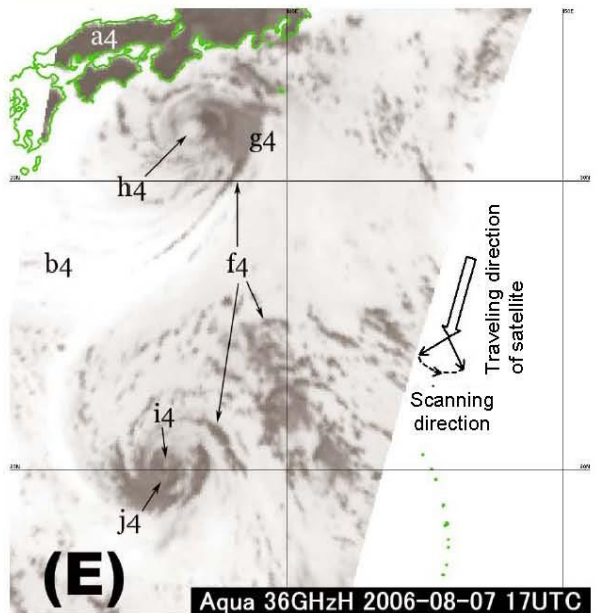
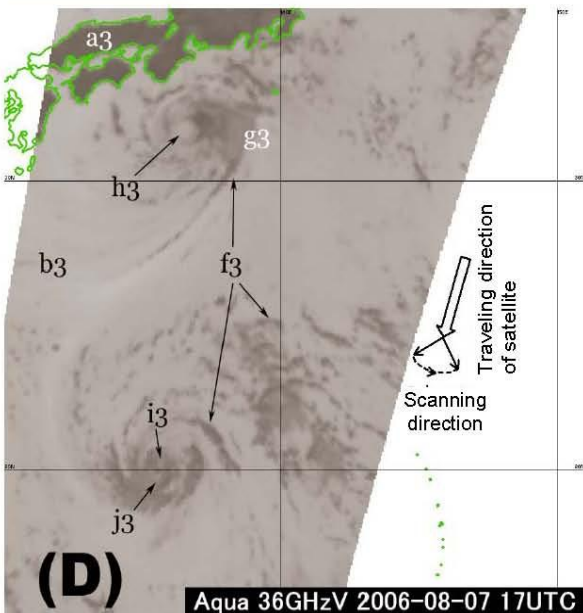
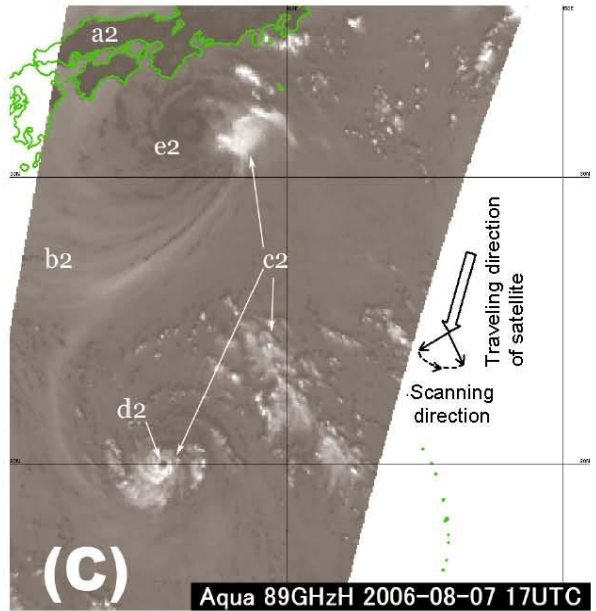
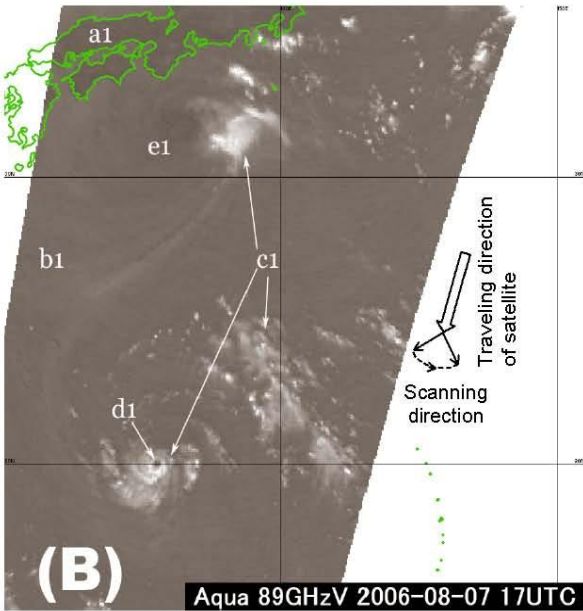


Figure 1-9 Differences in view between infrared and microwave images (17UTC, Aug. 7, 2006)

(A) Infrared image, (B) 89-GHz vertical polarization image, (C) 89-GHz horizontal polarization image, (D) 36-GHz vertical polarization image, and (E) 36-GHz horizontal polarization image

In each image, a darker (black) region indicates a region of higher brightness temperature, and a lighter (whiter) region indicates a region of lower brightness temperature.



location of the eye.

In images (D) and (E) of the 36-GHz band, both typhoons are increased in radiation temperature in the water cloud regions (e.g., f3 and f4), and are darker than the sea surface. The important point to note is that well-developed convection clouds (e.g., g3 and g4) look lighter than regions of only water clouds because many the ice particles in the upper water clouds decrease the brightness temperature, although the amount of decrease is not as significant as in the case of the 89-GHz band. In the 36-GHz band images, the eye of Typhoon No. 200607, which is difficult to locate in the 89-GHz band images, can be located as the center (h3 and h4) of a lower vortex of water clouds. The eye of Typhoon No. 200608 appears as an off-white region (i3 and i4) near the north side of the 20th parallel north of the equator. A difference in position of approximately 10 kilometers originates with a parallax error, which is described in the next section. Other white areas (j3 and j4), which are confusing, are observed on the south side of the 20 degrees north. Area i3 looks darker than area i4 with a great difference in radiation temperature between the vertical and horizontal polarizations. This suggests that areas of low brightness temperature of the region are the sea surface. On the other hand, no difference in radiation temperature between areas j3 and j4 is observed, which suggests that the decrease in radiation temperature is caused by scattering particles in an extremely well-developed cumulonimbus cloud. Like these examples, comparison of brightness temperature between the vertical and horizontal polarizations can avoid confusion.

#### **1.3.4 Important Points on Analysis with Microwave Imagery**

Because of the basic properties of microwaves, the 89-GHz and 36-GHz bands have the advantage that images taken with these bands provide information about areas under high-level clouds, which is unknown on infrared or visible images. As previously described, however, their main objects to be analyzed are different, so it is important to use the advantages of both bands to complement each other. However, images of these bands have the disadvantages described below, so infrared or visible images should be used, if necessary.

The altitude to be observed differs between the 89-GHz and 36-GHz bands. The 89-GHz band is used to observe active convection areas over the melting layer, while the 36-GHz band is for water clouds below the layer. If a disturbance such as a typhoon is observed using these bands, a broad area of water clouds can be observed with the lower-frequency band, while an area of active convection in the water clouds is observed with the other band.

This difference in the altitude to be observed between both bands exerts an influence mainly on analyses of typhoon eyes. Cloud walls surrounding a typhoon eye tend to be larger in higher altitude. Therefore, a typhoon eye is observed at a high altitude with the 89-GHz band, and the area of the eye is found to be larger than an area observed with the 36-GHz band (Figure 1-10). Using this low-frequency band, a typhoon eye is observed at a low altitude, and is found to be smaller in area

than one using the high-frequency band (Figure 1-10). However, the resolution of the 36-GHz band is lower than that of the 89-GHz band, and the outer edges of water clouds frequently appear as unclear, so comparison between both images is necessary for analysis.

Another important point to note is that as described in Chapter 1.2.4, a microwave imager observes the surface of the earth at an angle (incident angle of approximately 55 degrees) by conical scanning. In the location of a typhoon eye, a deviation is observed, as shown in Figure 1-11. This difference is called a parallax error. The parallax error of the 89-GHz band, the detection range of which is at a higher altitude than that of the 36-GHz band, is larger than that of the 36-GHz band. Naturally, a parallax error is produced even with the 36-GHz band, so it is necessary to correct these differences to the extent possible.

However, it is difficult to estimate the degree of the parallax error for each band because the altitude with the highest detection range of a band depends on the vertical structure of clouds or atmospheric profiles at any given time. Using the 89-GHz band, a satellite observes an area around the tropopause at a certain altitude distribution of scattering particles, producing a disparity of approximately 20 kilometers.

If an analysis finds a deviation in the location of the typhoon eye between the 89-GHz band and 36-GHz band images, the first cause to be suspected is a parallax error. To correct this, it is necessary to consider the traveling direction of a satellite on the orbit and the orientation of the sensor.

As mentioned so far, analyses using microwave images provide useful pieces of information, but they are not always effective. Concurrent use of infrared or visible images will produce better results. If analyses using infrared or visible images are difficult, a microwave image should be used to know the inner structure of disturbance. If a microwave image provides insufficient information, comparison with analytical results using infrared or visible images is necessary. To fill the information gap of each image, it is necessary to use the advantages of different types of images.

In closing, characteristics of the 89-GHz and 36-GHz bands are listed in Table 1-2. Based on the characteristics of microwave images described so far, the survey mentioned in Chapter 2 is conducted.



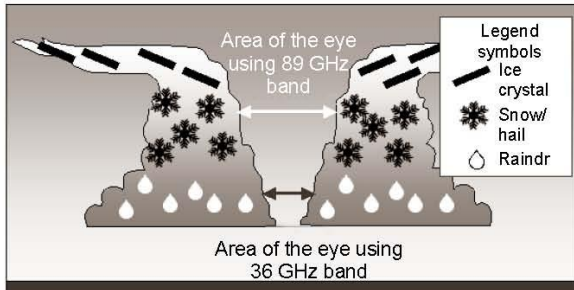


Figure 1-10 Schematic diagram of the observation altitude of a typhoon eye using different frequency bands

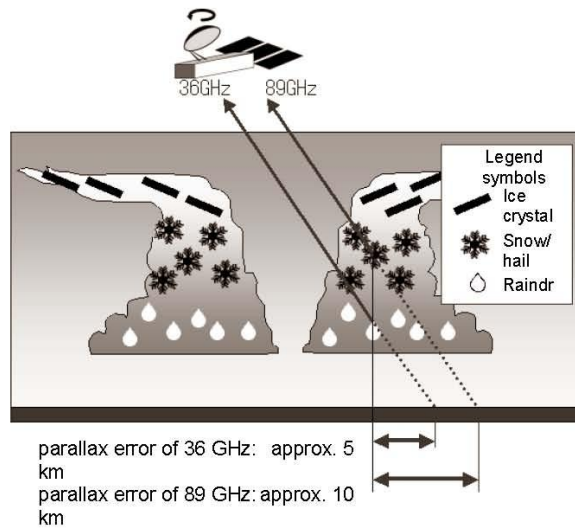


Figure 1-11 Schematic diagram of parallax error

Table 1-2 Characteristics of 89-GHz and 36-GHz bands

A circle sign shows a suitable characteristic for disturbance analysis for the frequency band.

An × sign shows an unsuitable or noteworthy characteristic for analysis for the frequency band.

36 GHz Band	89 GHz Band
<b>○ Can analyze the structure of a typhoon under high-altitude clouds</b>	
× Lower resolution compared with 89 GHz band	<b>○ Higher resolution compared with 36 GHz band</b>
<b>○ Suitable for detection of water clouds or precipitation areas</b>	<b>○ Suitable for detection of well developed convection clouds</b>
× Cannot clearly distinguish between land and clouds	△ Can track convection clouds over the land
	× Can confuse between cold sea surface and convection clouds
<b>○ Smaller parallax error compared with 89 GHz band</b>	× Larger parallax error compared with 36 GHz band
<b>○ Observe a smaller size of a typhoon eye at low altitude</b>	× Observe a larger size of a typhoon eye at high altitude

## 2. Tropical disturbance analysis using microwave imagery

### 2.1 Overview

Microwave imagery obtained with the AMSR-E sensor loaded on the Aqua polar orbiter has been available since June 2003. Taking this opportunity, the Analysis Division of the Meteorological Satellite Center has conducted research and technological development for application of such imagery to tropical disturbance analysis.

Analyses of typhoon eyes using microwave imagery have already been conducted by, for example, Lee et al. (2002), who provided qualitative information only. We focused our study on the development of an analytical method that is as quantitative as possible, and developed a new analytical method for typhoon eyes using microwave imagery. Our newly developed method was compared with the radar weather report method, such as RADOB, to study analytical parameters, such as precision.

### 2.2 Study Period

June 2003 to December 2005

### 2.3 Tropical disturbance to be analyzed

Our analysis targets are microwave imagery of tropical disturbance obtained during our study period. They are listed in Table 2-1.

### 2.4 Analysis items

- a. Pattern-specific occurrence rate using imagery

Different images are obtained for the same tropical disturbance between microwave imagery and visible/infrared imagery. In our study, therefore, we classified the cloud

Table 2-1 Tropical disturbance analyzed  
For the TC numbering, see Appendix 2 “Abbreviations.”  
Figures in parentheses indicate numbers that could be analyzed.

Year 2003

TC0007(2)	TC0017(6)	TC0029(2)
TC0011(1)	TC0020(12)	TC0030(1)
TC0012(8)	TC0021(8)	TC0031(15)
TC0015(1)	TC0025(1)	
TC0016(6)	TC0026(4)	

Year 2004

TC0003(14)	TC0015(8)	TC0027(2)
TC0004(8)	TC0016(1)	TC0031(12)
TC0006(4)	TC0018(8)	TC0032(6)
TC0007(7)	TC0019(5)	TC0033(8)
TC0008(3)	TC0020(7)	TC0034(11)
TC0009(8)	TC0021(16)	TC0035(11)
TC0010(8)	TC0022(8)	TC0037(7)
TC0011(11)	TC0023(1)	TC0040(5)
TC0012(4)	TC0024(16)	
TC0013(8)	TC0025(4)	

Year 2005

TC0001(5)	TC0009(7)	TC0017(11)
TC0002(6)	TC0010(3)	TC0018(8)
TC0003(8)	TC0011(10)	TC0019(5)
TC0004(13)	TC0012(10)	TC0020(15)
TC0005(12)	TC0013(7)	TC0021(8)
TC0006(7)	TC0014(13)	TC0022(8)
TC0007(6)	TC0015(12)	TC0023(7)
TC0008(5)	TC0016(2)	

pattern of tropical disturbance on microwave imagery into three empirical types, and studied the occurrence rate of each type.

b. Analytical precision for tropical disturbance

The distance between the eye of a tropical disturbance analyzed using microwave imagery and that using visible/infrared imagery, and their latitude and longitude errors are studied. Using RADOB reports that provide precise positional information as independent data, distances from eyes obtained by analysis on microwave imagery and latitude and longitude errors are studied to determine the precision of our analytical method.

c. Comparison of imagery between microwave and visible/infrared

Measurement items in traditional tropical disturbance analysis using visible and infrared imagery include “eye precision.” This information suggests the diameter of an area in kilometers, in which the eye of a tropical disturbance exists with a 90 percent probability. In our study, using the traditional measurement method of eye precision as a guide, a new measurement method suitable for precision of our microwave imagery analysis is defined, and measurement is performed using the new method. Our newly defined item is called the eye analysis size in this document. Values obtained using microwave imagery are compared with those obtained using traditional visible/infrared imagery.

On a man-machine interface, a qualitative evaluation is also performed on microwave imagery and visible/infrared imagery to check which imagery provides clearer and easier-to-understand information.

## **2.5 Analytical procedures**

A microwave image of a tropical disturbance is analyzed in the following steps and order: pattern selection; eye analysis; measurement of eye analysis size; and comparison between microwave imagery and visible/infrared imagery (Figure 2-1).

In pattern selection, a cloud pattern in microwave imagery is determined based on the criteria of the chart in Figure 2-1. After this step, an “eye analysis” and “eye analysis size” measurement are performed based on the methods for the selected pattern. If a cloud pattern is found to be “unknown,” these analyses are not performed.

“Comparison between microwave imagery and visible/infrared imagery” offers seven options, among which an analyzer selects an appropriate one. The options and selection conditions are listed in Table 2-2.

Based on the characteristics and resolution of channels, 89 GHz and 36 GHz are selected as analysis channels. Vertical polarization is used because of its high emissivity. Basically, only images of tropical disturbance over the sea are analyzed. Images of disturbance over the land are not analyzed because the decrease in contrast between the disturbance and the land surface resulting from a higher

emissivity from the land surface than from the sea surface often makes analyses difficult. A quality control (QC) value of 2 degrees is set as a threshold value for statistical work of analytical results to determine the distance between two points and the latitude and longitude errors of two points. If the latitude and longitude error of two points is 1.9 degrees, the data are accepted. If the error is 2.1 degrees, the data are rejected, for example. This acceptance/rejection criterion is set so as not to analyze the wrong data in the case of more than one disturbance in close proximity to each other. The value is based on a distance of about 2 degrees at 20 degrees north latitude, which is converted from an accuracy of constant 175 kilometers for the Cb cluster pattern in traditional visible/infrared imagery analysis.

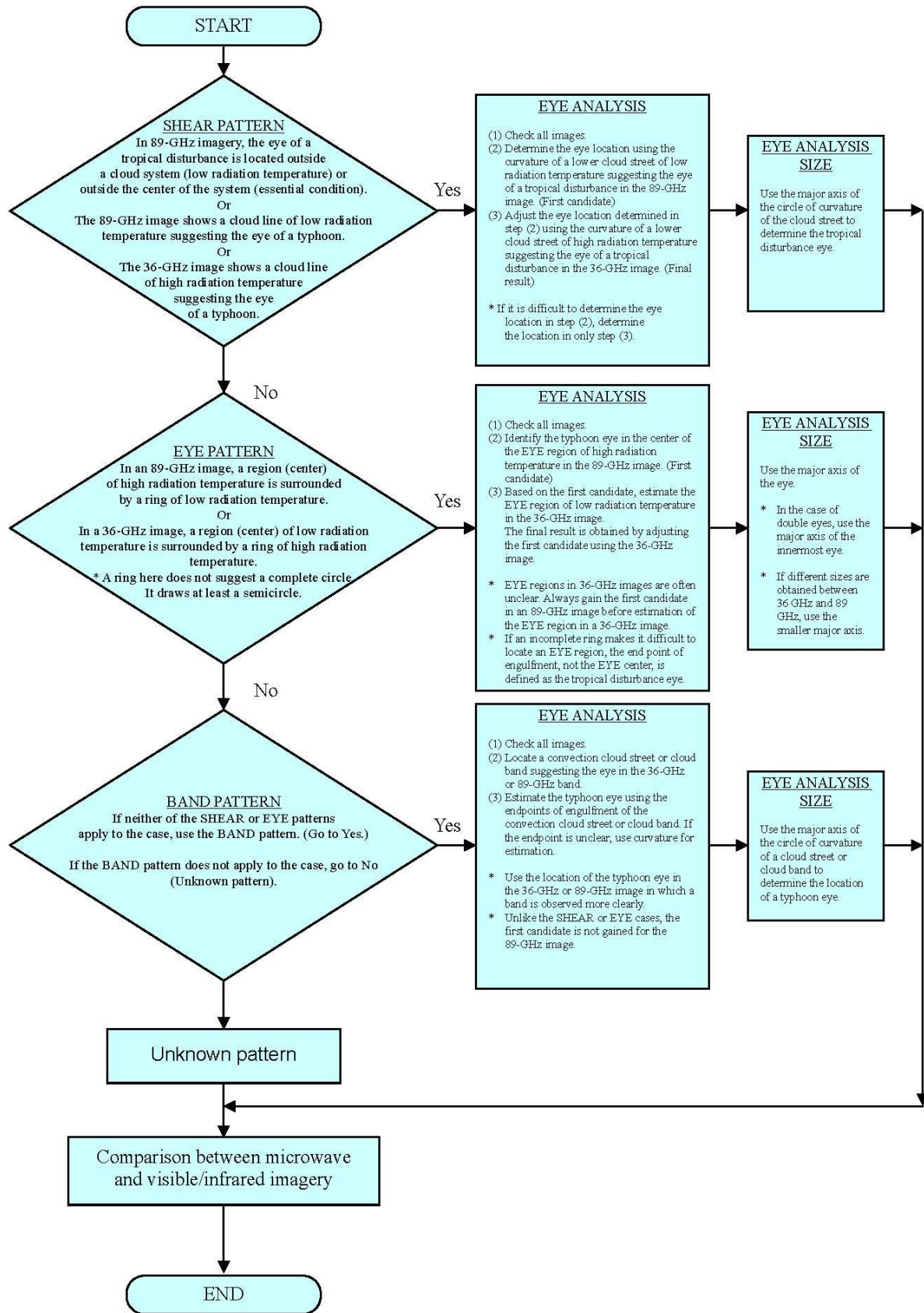


Figure 2-1 Flow chart of analytical procedures

Table 2-2 Options and criteria for comparison between microwave and visible/infrared imagery

Option	Condition	Remarks
Microwave imagery is clearer.	The eye is located clearly in the EYE pattern on microwave imagery. Other than EYE pattern in visible/infrared imagery	
	The eye is clearly located in the BAND or EYE pattern in microwave imagery. Difficult to locate the typhoon eye in visible/infrared imagery	
Microwave imagery is slightly clearer.	EYE pattern in microwave imagery The eye is clearly located in other than the EYE pattern in visible/infrared imagery.	Clearness of eye location in visible/infrared imagery is based on the ability of location of a typhoon eye without seeing moving images.
	The typhoon eye is clearly located in a clear BAND in other than the EYE pattern in microwave imagery. Typhoon eye is located unclearly in visible/infrared imagery	
Microwave and visible/infrared imagery are both unclear.	Unknown pattern in visible/infrared and microwave imagery, and difficult to locate the typhoon eye	Select in the case of UNDEFINED for visible/infrared imagery or unknown pattern for microwave imagery. Useful for SHEAR on extremely unclear images
Microwave and visible/infrared imagery are both clear.	EYE in both visible/infrared and microwave imagery	
Visible/infrared imagery is slightly clearer.	The typhoon eye is located unclearly in BAND or SHEAR in microwave imagery. The eye is clearly located in visible/infrared imagery.	The eye is located unclearly in both visible/infrared and microwave imagery, but can be located in visible/infrared imagery.
Visible/infrared imagery is clearer.	Unknown pattern in microwave imagery and unclear typhoon eye location Clear or slightly clear eye location in visible/infrared imagery	Select in the case of unclear cloud streets in the SHEAR pattern in microwave imagery.
Unknown	Peculiar images, and not included in the above classification	

\* Use the Dvorak method as the analytical method for tropical disturbance in visible/infrared imagery.

## 2.6 Cloud patterns in microwave imagery

In our study, a suitable cloud pattern in microwave imagery is selected among the following three options.

- a. SHEAR pattern
- b. EYE pattern
- c. BAND pattern

These are patterns empirically determined based on convection cloud streets and eyes of tropical disturbances. Their names are the same as those of the Dvorak method, but given slightly different definitions for our classification because vision in microwave imagery differs from that in visible/infrared imagery (Figure 2-1). Characteristics of the three patterns and measurement methods of “Eye Analysis” and “Eye Analysis Size” are described using actual images.

### a. SHEAR pattern

A schematic diagram of the SHEAR pattern is shown in Figure 2-2a. A characteristic of this pattern is that the eye of a tropical disturbance is away from the cloud zones where disturbances are developed. Cloud zone A is a cloud system of a tropical disturbance, and appears as a well-developed cloud zone of low radiation temperature on 89-GHz imagery. Cloud zone B is a frontal cloud band. Although this band is not always accompanied, it is often accompanied in the northern part of the mid-latitude region. Convection cloud street C is seen with relatively high

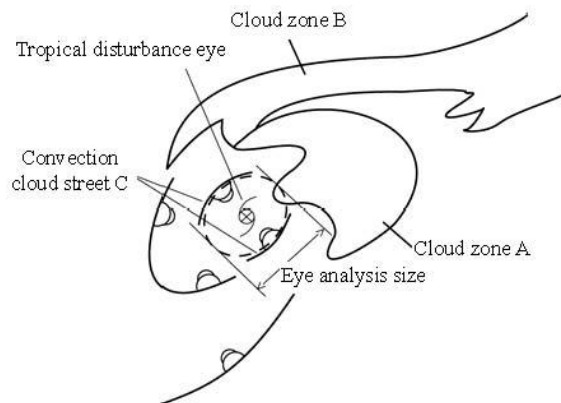


Figure 2-2a Schematic diagram of the SHEAR pattern

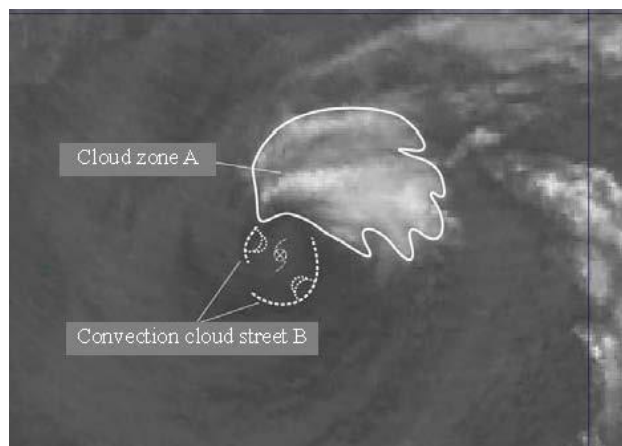


Figure 2-2b TC0004 89 GHz  
Taken at 17UTC, June 8, 2005  
Eye location: 26.6N 135.1E



Figure 2-2c TC0004 36 GHz  
Taken at 17UTC, June 8, 2005  
Eye location: 26.6N 135.1E

clearness on 36-GHz imagery. To locate the eye, a cloud street that may suggest an eye, like convection cloud street C, is sought and the eye is located by locating the center of the circle of curvature (dotted line of the ellipse in Figure 2-2a) formed by the cloud street. As the eye analysis size, measure the length of the major axis of the circle of curvature.

Figure 2-2b shows a cloud pattern observed with the 89-GHz band. Cloud zone A is a cloud system of a tropical disturbance or a well-developed cloud zone of low brightness temperature. On the south side of this zone, convection cloud street B of high radiation temperature is observed. Cloud streets that may suggest the eye are shown by dotted lines. However, brightness temperature of the cloud streets is nearly the same as that of the sea surface, resulting in a low contrast between them. Therefore, they cannot be distinguished from the sea surface. The eye suggested from these streets is also shown. This is the candidate for the tropical disturbance eye.

In the 36-GHz imagery, the amount of microwaves emitted from the sea surface is small, so a convection cloud street is easily identifiable. Among convection cloud streets on the image, a combination of those that may suggest the eye is selected. An example of this is shown in Figure 2-2c. Using the calculated curvature of the clouds, the eye location is estimated. If this location is different from that in the 89-GHz imagery, use the figure of the 36-GHz imagery because its parallax error is smaller (final result). The length of the major axis of the circle of curvature (dotted line ellipse) formed by the selected convection cloud streets is measured as the eye analysis size.

#### b. EYE pattern

In microwave imagery, there are two possible cases: i. the complete-ring eye (Figure 2-3a), and ii. the incomplete-ring eye (Figure 2-4a). Even in the latter case, if a cloud band stretches at least halfway around the eye, the EYE pattern can be applied.

##### i Complete-ring eye

Figure 2-3a shows a schematic diagram of the “complete-ring EYE” pattern. A cloud zone takes the shape of a complete ring, which make eye analysis easy.



In an 89-GHz band image (Figure 2-3b), cloud zone A of low brightness temperature, which takes the shape of a ring, is the major characteristic of this pattern. The eye is in an area of high brightness temperature shown by a dotted line circle near the center of the cloud zone. The center of this area is defined as the eye (candidate). The eye analysis size is defined as the diameter of the eye or the major axis, so in this figure, the diameter of the dotted line circle is measured.

In the 36-GHz band image of Figure 2-3c, the eye is in an area of low brightness temperature in the central part of the cloud zone, and the center of this area is the eye of the disturbance. If the eye in the 36-GHz image is clearly seen, and differs in location from the eye in the 89-GHz image, the eye location in the 36-GHz band, which is less affected by parallax, is accepted as the eye of the disturbance (final result). If the eye in the 36-GHz image is unclear, the eye location in the 89-GHz image is accepted as the eye location of the disturbance. The eye analysis size is the diameter or major axis of the eye. In Figure 2-3c, the length of the major axis of the dotted-line ellipse is measured. This value is compared with that of the 89-GHz image, and a smaller one is accepted as the final eye analysis size.

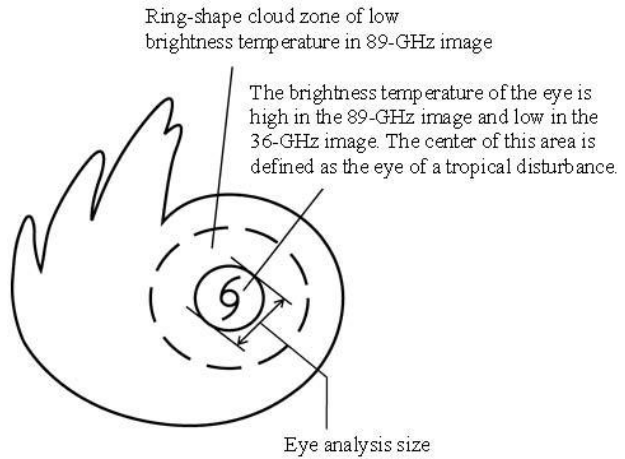


Figure 2-3a Pattern of complete-ring EYE

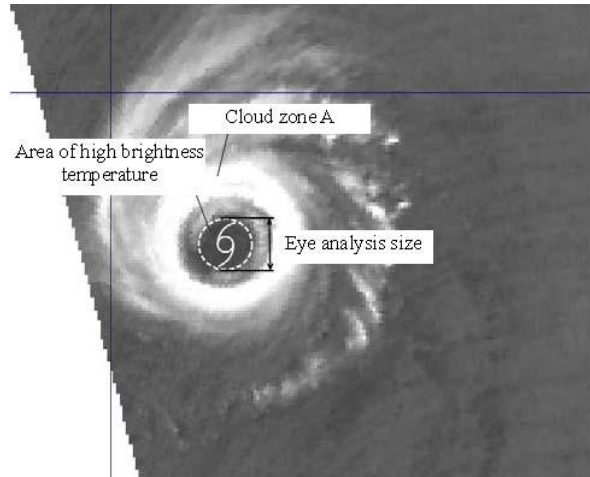


Figure 2-3b TC0003 89 GHz  
Taken at 04UTC, April 13, 2004  
Eye location: 17.5N 131.2E

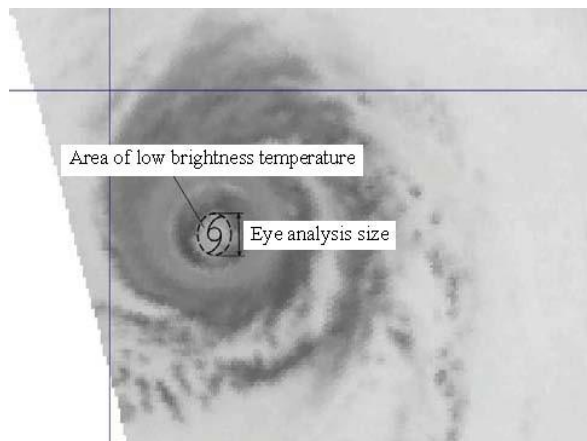


Figure 2-3c TC0003 36 GHz  
Taken at 04UTC, April 13, 2004  
Eye location: 17.5N 131.2E

ii Incomplete-ring eye

Figure 2-4a shows a schematic diagram of the “incomplete-ring EYE” pattern. Unlike the complete-ring pattern, the main characteristic of the pattern is that a cloud band does not form a complete ring, and is swirling. This pattern is often observed clearly in 89-GHz images and is often confused with the EYE pattern, which has an ambiguous ring structure in 36-GHz images.

An example of 89-GHz images is shown in Figure 2-4b. An area of low brightness temperature (cloud zone A) surrounded by a white solid line takes the shape of an “incomplete ring.” Area B of high brightness temperature in the central portion of zone A is the eye. The center of this area is defined as the eye of the disturbance (candidate). The length of the major axis of the dotted-line ellipse is measured as the eye analysis size.

Figure 2-4c is a 36-GHz image in which the eye is an area of low brightness temperature (dotted-line ellipse) in the central portion of a cloud zone of high brightness temperature. The center of this eye is the eye of the disturbance. If the eye location is different between the 36-GHz and 89-GHz images, which is caused by parallax, the eye location of the 36-GHz image is accepted (final result). If the eye is not observed more clearly in the 36-GHz image than in the 89-GHz image, the eye location in the high-frequency image is accepted (the final result). The eye analysis size is the major axis of the eye (dotted-line ellipse). This value is compared with that of the 36-GHz image, and the smaller one is accepted as the final eye analysis size.

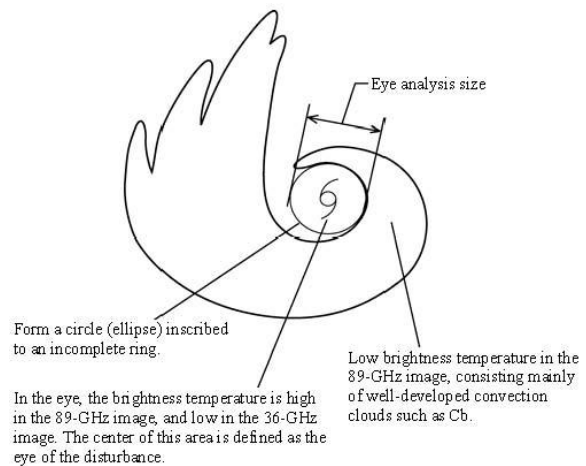


Figure 2-4a Incomplete-ring EYE pattern

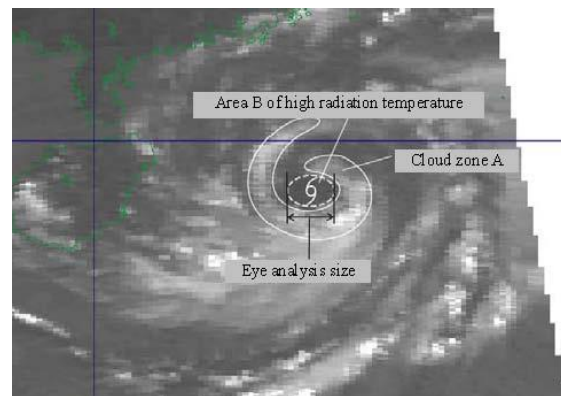


Figure 2-4b TC0006 89 GHz  
Taken at 06UTC, Aug. 24, 2003  
Eye location: 19.1N 113.7E

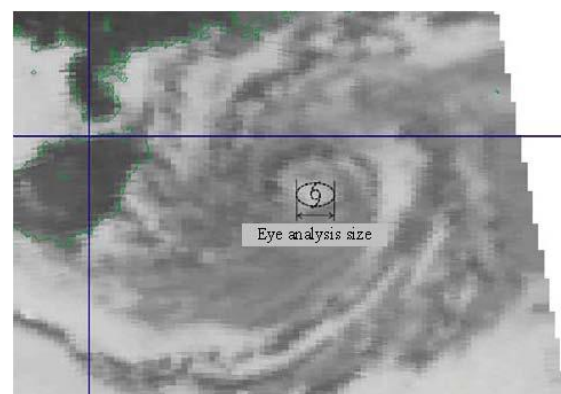


Figure 2-4c TC0006 36 GHz  
Taken at 06UTC, Aug. 24, 2003  
Eye location: 19.1N 113.7E

## BAND pattern

In sharp contrast to the SHEAR pattern, in the BAND pattern, the eye of the disturbance is in a cloud system. In contrast to the EYE pattern, in the BAND pattern, no eye is formed or an arc is with its length being less than half that of a complete ring is formed due to in-progress formation. Compared with the SHEAR and EYE patterns, the BAND pattern has no clear convection cloud streets, and there are often scattered convection clouds. Before an eye analysis, it should be checked whether a cloud zone of low brightness temperature in an 89-GHz band image or one of high brightness temperature in a 36-GHz band image has a curvature that suggests an eye or takes the shape of a band.

Figure 2-5a shows a schematic diagram of the BAND pattern. Cloud zone A is a cloud system of a tropical disturbance, which does not always exhibit low brightness temperature in 89-GHz images. If it consists mainly of water clouds, the cloud system appears as a clear area of high brightness temperature in 36-GHz images. Convection cloud street B is a cloud street that suggests the eye in a tropical disturbance system. The circle of curvature formed by this cloud street is the eye of the disturbance. The length of the major axis of this circle is measured as the eye analysis size.

Figure 2-5b shows an 89-GHz image of the BAND pattern, in which cloud zone A surrounded by a dotted line shows the cloud system of a disturbance. In this example,

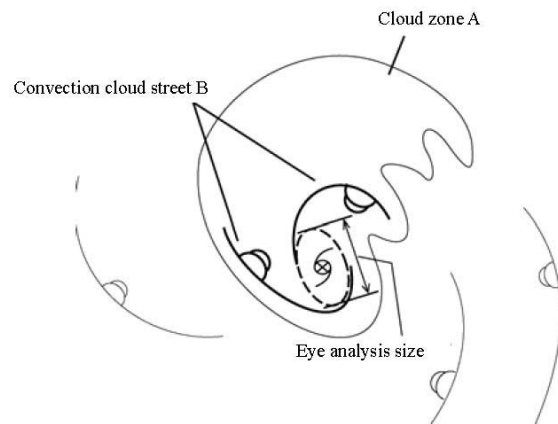


Figure 2-5a BAND Pattern

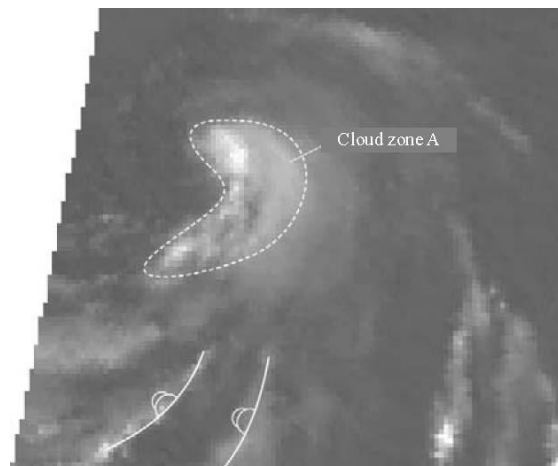


Figure 2-5b TC0008 89 GHz  
Taken at 18UTC, June 11, 2004  
Eye location: 13.7N 112.2E

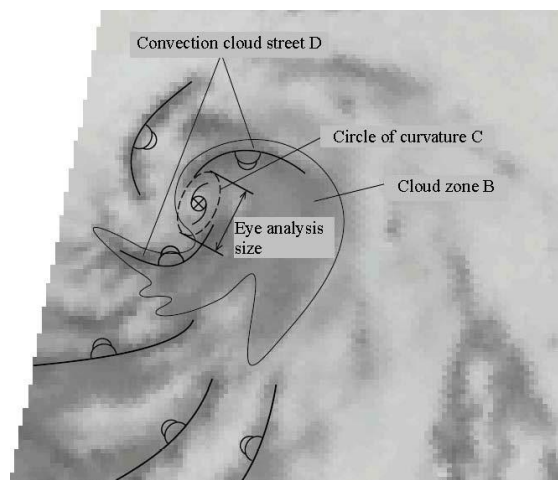


Figure 2-5c TC0008 36 GHz  
Taken at 18UTC, June 11, 2004  
Eye location: 13.7N 112.2E

clouds of low brightness temperature do not appear as dense cloud areas, and only a small portion of clouds in the image are sufficiently developed. In the image, the cloud system does not contain a cloud street that suggests the eye.

Figure 2-5c shows a 36-GHz image, in which cloud system B contains convection cloud street D that suggests the eye. The center of the circle of curvature C formed by this cloud street is the eye of the disturbance. The length of the major axis of this circle is measured as the eye analysis size.

## 2.7 Study results

The study results are described according to each item.

### a. Pattern-specific occurrence rate using microwave imagery

In our study, the EYE pattern accounts for 57.3 percent of the total, suggesting an extremely high occurrence rate of the pattern (Figure 2-6).

Table 2-3 lists the combination occurrence rates of patterns of tropical disturbance in visible/infrared imagery and the pattern of microwave imagery for the same observation time. Analysis times for visible/infrared imagery and those for microwave imagery were compared, and the number of comparable cases was found to be 161. The time interval for analysis of visible/infrared imagery is 6 hours in the case of tropical cyclones that require issuance of gale warnings, and 3 hours in the case of typhoons. Both cases are included in our study. When the SHEAR pattern is found on visible/infrared imagery, the same pattern is frequently found on microwave imagery. However, concerning the other patterns on visible/infrared imagery, the EYE pattern is the majority pattern on microwave imagery. Unknown patterns found on microwave imagery are not listed because the analysis time was not the time for typhoon analysis, or data were rejected based on the quality control threshold value of a latitude/longitude error of more than 2 degrees, as described in Chapter 2.5.

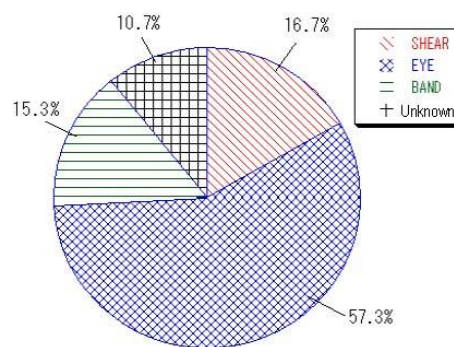


Figure 2-6 Pattern specific occurrence rates for a total of 466 cases

Table 2-3 Occurrence rates in a combination of patterns for visible/infrared and microwave imagery  
IRVIS refers to infrared and visible. MW refers to microwave. Total, 161 cases  
Each figure is the proportion of each MW pattern for each IRVIS pattern.

	IRVIS BAND	IRVIS B-EYE	IRVIS EMBED	IRVIS EYE	IRVIS SHEAR	IRVIS CB-Cluster
MW SHEAR	3.5	4.8	0.0	0.0	71.4	22.7
MW EYE	64.9	95.2	100.0	100.0	14.3	40.9
MW BAND	31.6	0.0	0.0	0.0	14.3	36.4

(Unit: %)

b. Analysis precision for tropical disturbance

i. Frequency distribution of eye distance

Figure 2-7 shows occurrence rates of eye distances between visible/infrared and microwave imagery based on the eye pattern.

In this figure, the rate columns of all types are piled up into a single column, as shown in the figure. No data are available for unknown patterns on microwave imagery because no eye analysis is performed on these patterns. The chart shows the highest frequency of distances of not less than 20 and less than 30 kilometers. The longer the eye distance, the less the frequency. Eye distances of not less than 100 kilometers account for 2.5 percent.

The occurrence rates of the EYE pattern are high at an eye distance of not more than 100 kilometers.

Figure 2-8 shows the occurrence rates of eye distances between RADOB reports and microwave imagery based on the eye pattern.

In RADOB reports, if a disturbance is observed at more than one radar site, data are reported by site. Even if more than one radar caught the same disturbance, we use both data. Times that match those of microwave imagery are extracted, so that a total of 71 cases are prepared. The results show the same tendency for eye distance between visible/infrared and microwave imagery (Figure 2-7). However, concerning the eye distance between visible/infrared and microwave imagery:

- The highest occurrence rate at a distance of not less than 20 to less than 30 kilometers.

And concerning the eye distance between microwave imagery and RADOB reports:

- The highest occurrence rate at a distance of not less than 10 to less than 20 kilometers.

The eye difference between visible/infrared and microwave imagery is smaller than that between microwave imagery and RADOB reports, which suggests a higher precision of comparison with RADOB reports. Based on its analytical precision, results of comparison with RADOB data are also

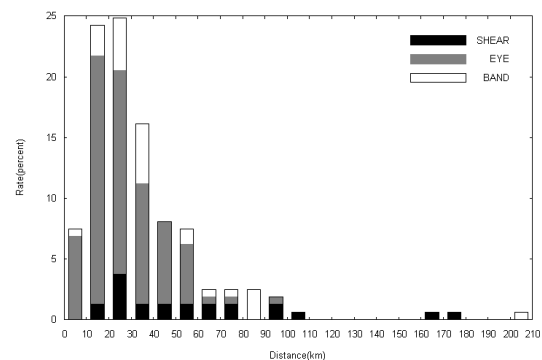


Figure 2.7 The horizontal axis indicates the eye distance between visible/infrared and microwave imagery. The vertical axis indicates the occurrence rate. Total, 161 cases

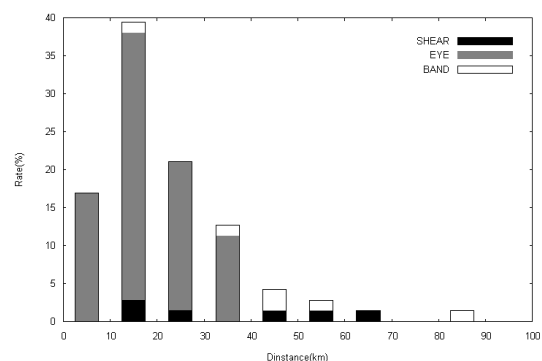


Figure 2-8 The horizontal axis indicates the eye distance between microwave imagery and RADOB reports. The vertical axis shows the occurrence rate. Total, 71 cases

acceptable.

ii. Latitude/longitude error distribution

Figure 2-9 shows the distribution of tropical disturbance eyes on visible/infrared imagery based on tropical disturbance eyes on microwave imagery. The distribution is created by plotting a value gained by subtracting (the microwave eye location) from (the visible/infrared eye location) on each latitude and longitude. Within  $\pm 0.3$  degrees, 66 percent of the data are distributed. Figure 2-10 is prepared by plotting a value gained by subtracting (the microwave eye location) from (the RADOB eye location) on each latitude and longitude. Within  $\pm 0.3$  degrees, 80 percent of the data are distributed. Errors of not less than one (1) degree are not observed in Figure 2-10, but are observed in Figure 2-9. These errors are produced because “off-target” analyses on eye location were performed. The use of microwave imagery can decrease the number of such errors.

c. Comparison between microwave and visible/infrared imagery

Figure 2-11 shows comparison between accuracy (eye precision) in visible/infrared imagery and eye analysis size in microwave imagery. For visible/infrared imagery, a range of 40 to 60 kilometers is observed frequently, while a range of 20 to 40 kilometers is observed frequently for microwave imagery. This means that it is easier to locate the eye of a disturbance using microwave imagery.

On the assumption that eye locations of

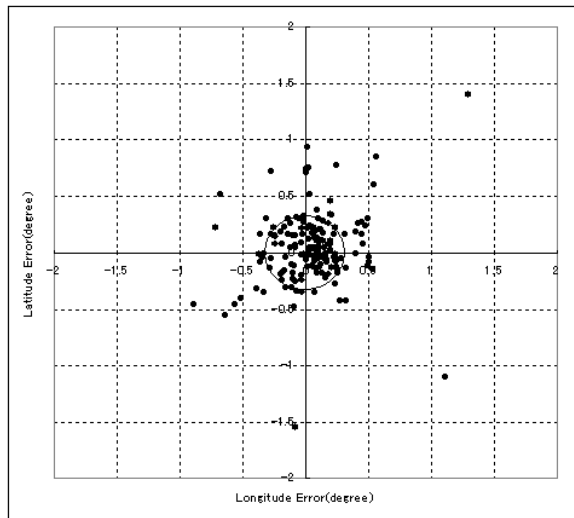


Figure 2-9 Scatter diagram of eye location of visible/infrared imagery based on microwave imagery  
The origin is the eye location of disturbance on microwave imagery. Plotted data show eye locations on visible/infrared imagery. The circle has a diameter of 0.3 degrees. Total, 161 cases

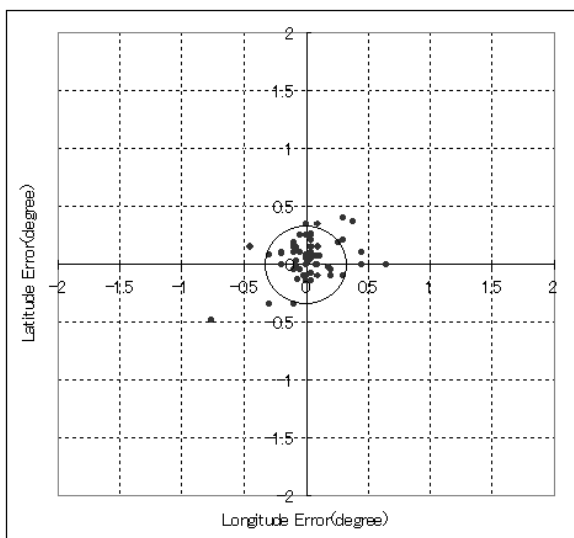


Figure 2-10 Scatter diagram of eye location of RADOB data based on microwave imagery  
The origin is the eye location of disturbance on microwave imagery. Plotted data show eye locations on RADOB reports. The circle has a diameter of 0.3 degrees. Compared with Figure 2-8, the data are less scattered. Total, 71 cases



RADOB reports are correct, the probability that the eye distance between microwave imagery and RADOB reports is not more than the eye analysis size is 92 percent. This means that within the area of the eye analysis size of microwave imagery, there are 92 percent of the eyes on RADOB reports. The eye analysis size carries nearly the same meaning as that for accuracy (eye precision) for visible/infrared imagery.

Figure 2-12 shows the comparison results of the imagery type for an operator to analyze a tropical disturbance with ease between microwave and visible/infrared. Items of “Microwave imagery is clearer” and “Microwave imagery is slightly clearer” account for more than 50 percent of the total.

This means that operators could analyze disturbance eyes more easily using microwave imagery. As an example, Figure 2-13 shows an image of TC0007 taken at 18UTC, June 6, 2004. At that time, a gale warning was issued, but a typhoon was not generated. The Analysis Division of the Meteorological Satellite Center was conducting an early-stage Dvorak analysis. The organized Cb cluster pattern is used for traditional operational analysis using visible/infrared imagery. Because of dense high-altitude clouds across an image, it is difficult to locate an eye without seeing a moving image. In microwave imagery, an at least one half of a ring of cloud is observed in an 89-GHz image, and a complete ring of cloud is observed in a 36-GHz image. The pattern is the microwave EYE pattern. As this example shows, eye analysis work is easier using microwave imagery.

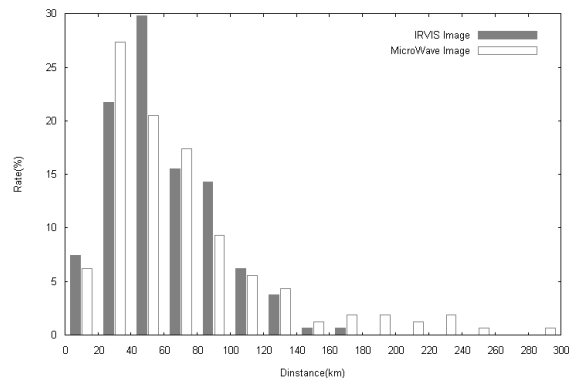


Figure 2-11 Occurrence rates of accuracy (eye precision) for visible/infrared imagery and eye analysis size for microwave imagery for intervals of 20 kilometers Total, 161 cases

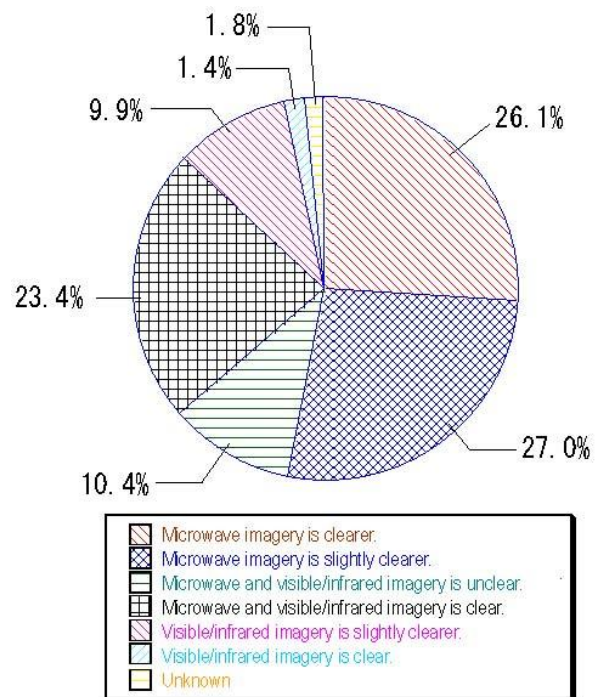


Figure 2-12 Comparison of ease of eye analysis work

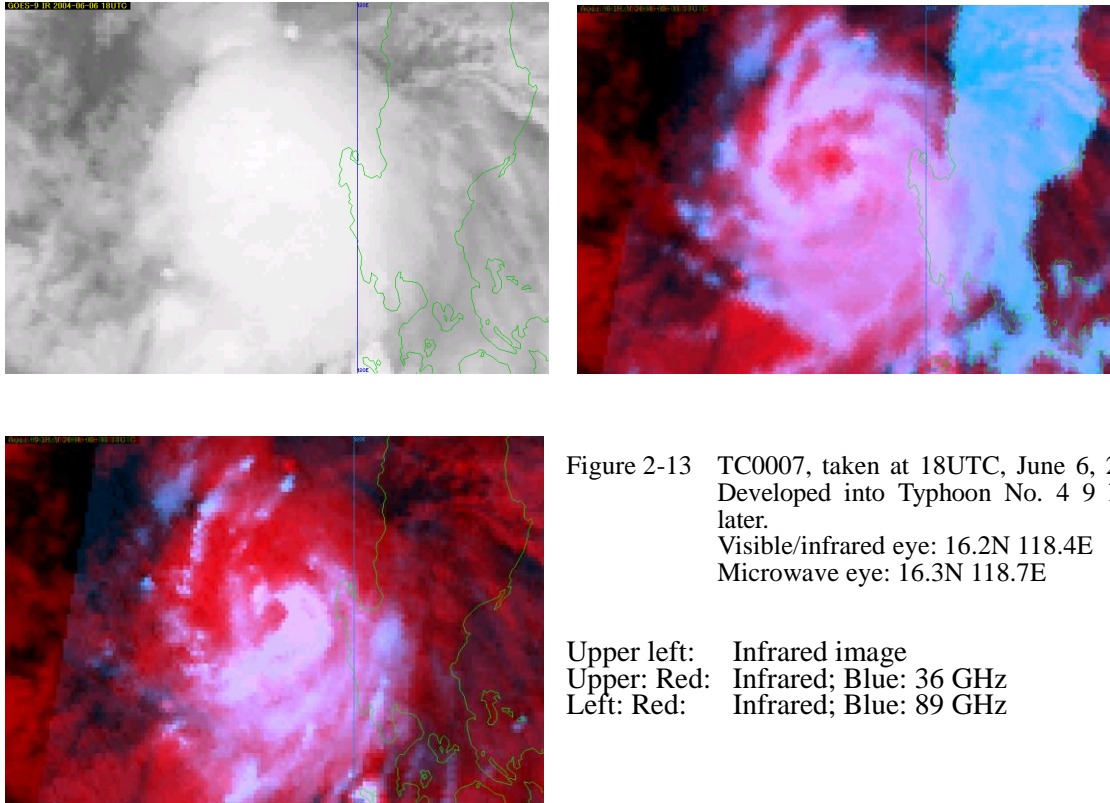


Figure 2-13 TC0007, taken at 18UTC, June 6, 2004.  
 Developed into Typhoon No. 4 9 hours  
 later.  
 Visible/infrared eye: 16.2N 118.4E  
 Microwave eye: 16.3N 118.7E

Upper left: Infrared image  
 Upper: Red: Infrared; Blue: 36 GHz  
 Left: Red: Infrared; Blue: 89 GHz

## 2.8 Discussion

### a. Observation frequency per day

A problem of tropical disturbance analysis using microwave imagery is the low frequency of observation. Satellite MTSAT-1R observes the northern hemisphere of the earth twice an hour, which comes to 48 times in 24 hours. Satellite AMSR-E observes an area at a longitude of 100 to 180 degrees about 8 times per day. Because of its low swath width, approximately 1400 kilometers, the number of times that the satellites passes over a tropical disturbance with a size of approximately 1000 kilometers is very small, producing a small number of images taken. This problem can be solved by using many data obtained with polar orbiting satellites; however, at the present, in the number of observation times, a geostationary meteorological satellite, which can observe an object twice an hour and whose moving images can be used for eye analyses, compares favorably with the microwave satellite.

### b. Resolution

The resolution of Satellite MTSAT-1R is 4 kilometers on infrared imagery and 1 kilometer on visible imagery. The resolution of AMSR-E is 5 kilometers for the 89-GHz band, and 11 kilometers for the 36-GHz band. In resolution, the latter satellite compares unfavorably with the former.



c. Pattern classification

Selection between the SHEAR and BAND patterns depends frequently on the operator. The BAND pattern is selected if a phenomenon is not classified into the SHEAR or EYE pattern. Because it is passively selected, adoption of the BAND pattern depends on an operator who judges the possibility of analysis using the SHEAR pattern. It is a future task to define the BAND pattern more clearly.

d. Eye analysis precision

As described in Chapter 1, a cloud zone observed with the AMSR-E sensor that uses a conical scan mode has a certain degree of parallax with respect to the ground surface. In our study, to reduce this difference to the extent possible, the final result of eye location is determined using 36-GHz images, which are lower in parallax than 89-GHz images. However, 36-GHz images still have some degree of parallax, and this fact should be kept in mind during eye analysis using microwave imagery.

On the assumption that eye locations in RADOB reports are reliable, eye locations identified using microwave imagery are more precise than those using visible/infrared imagery, according to our study results. The eye distance between RADOB reports and microwave imagery is found to be at least 10 and less than 20 kilometers with high frequency, and less than 10 kilometers with low frequency. These margins of error are unavoidable in the analytical results of microwave imagery.

d. Automation of eye analysis

According to our study, in comparison with visible/infrared imagery, on microwave imagery, the EYE pattern is more frequently observed, and an eye analysis is easier. It seems that this fact is advantageous only when an operator conducts an eye analysis on the man-machine interface. A cloud of a ring of low or high radiation temperature that clearly suggests the eye is useful for automatically locating eyes using software applications.

e. Observation site for three patterns for microwave imagery

Because in our study, eye analyses are performed on all of the three patterns, excluding unknown patterns, whether observation points have any unique characteristics for each pattern is checked, which found no major difference. In order to observe the generation of a tropical disturbance at an earlier stage, information on sites of tropical disturbance generation is important, which we have not studied. This merits further research.

## 2.9 Summary

When a tropical disturbance is observed on microwave imagery, the occurrence rate of the EYE pattern accounts for 60 percent of the total, which shows that it is the majority pattern among all. Many patterns other than the EYE pattern on visible/infrared imagery are found to be the EYE pattern on microwave imagery. Concerning eye analysis precision using microwave imagery, eye locations analyzed using microwave imagery are found to be approximate values of RADOB reports. An eye

analysis using microwave imagery is found to be more precise than that using only visible/infrared imagery.

## References

- Norihisa Usui, Yukio Kurihara and Akiko Shoji, 2003: QuikSCAT Verification Study and Objective Analysis using the Variation Method on Ocean Winds, *Weather Service Bulletin*, 70.2, P25-39.
- Koji Kato, Makoto Nishida, Masayuki Yamamoto, Naoyuki Shimizu and Akihiro Kikuchi, 2004: Tropical Disturbance Analysis System, *Meteorological Satellite Center Technical Note No. 44*, Meteorological Satellite Center, P31-38.
- Shuji Nishimura, 2006: 2-9 Tropical Disturbance Analysis, 2006 Special Issue of *Meteorological Satellite Center Technical Note Comprehensive Report of MSC System*, Meteorological Satellite Center, P145-153.
- Tadahiro Hayasaka (ed) 1996: *Remote Sensing of the Atmosphere Using Microwave Radiometry*, Meteorological Study Note, 187, PP196.
- Masaya Hirohata, 2004: Chapter 5 Use Various Types of Satellite Data, Analyze and Use Meteorological Satellite Images --Tropical Cyclones--, Meteorological Satellite Center, P102-107.
- Yukio Fujita and Takeshi Hagiwara, 2000: Chapter 1 Meteorological Satellite Observation of Typhoons, *Meteorological Study Note*, 197, P1-75.
- Grody, N. C., 1993: *Remote Sensing of the Atmosphere from Satellite Using Microwave Radiometry*, *Atmospheric Remote Sensing by Microwave Radiometry* (eds. M. A. Janssen), John Wiley & Sons, New York, P37-90.
- Kidder, Stanley Q., Mitchell D. Goldberg, Raymond M. Zehr, Mark DeMaria, James F. W. Purdom, Christopher S. Velden, Norman C. Grody, and Sheldon J. Kusselson, 2000: Satellite Analysis of Tropical Cyclones Using the Advanced Microwave Sounding Unit (AMSU), *Bulletin of the American Meteorological Society*, 81, 1241-1259.
- Lee, Thomas F., Francis J. Turk, Jeffrey Hawkins, and Kim Richardson, 2002: Interpretation of TRMM TMI Images of Tropical Cyclones, *Earth Interactions*, 6, P1-17.
- NASA, 1987: High Resolution Multi-frequency Microwave Radiometer, *Earth Observing System Volume IIe, Instrument Panel Report*, NASA, Washington D.C., P59.
- Randall J. Alliss, Sethu Raman and Simon W. Chang, 1992: Special Sensor Microwave / Imager (SSM/I) Observations of Hurricane Hugo (1989), *Monthly Weather Review*, 120, P2723-2737.
- Randall J. Alliss, Glenn D. Sandlin, Simon W. Chang and Sethu Raman, 1993: Applications of SSM/I Data in the Analysis of Hurricane Florence (1988), *Journal of Applied Meteorology*, 32, P1581-1591.
- Spencer, Roy W., H. Michael Goodman, Robbie E. Hood, 1989: Precipitation Retrieval over Land and Ocean with the SSM/I: Identification and Characteristics of the Scattering Signal, *Journal of*

Atmospheric and Oceanic Technology, 6, 254-273.

## Appendix 1 Satellites and Sensors

The following is a description of abstracted, revised and edited information about satellites and sensors provided from the appendix of separate report No. 53 of the Numeric Prediction Division.

- The following satellites and sensors are relevant to our report, and do not cover all sensors loaded on to the satellites.
- Shaded areas are concerned with satellites that have not been launched and may be subject to their program review or change in the future.
- Abbreviations in the tables are as follows: IR: Infrared; MW: Microwave; VIS: Visible; VN: Visible-Near infrared; SW: Short wavelength infrared; WV: Water vapor channel of stationary satellite; -S: Sounder; -I: Imager; -IS: Imager/sounder; and -HS: Hyperspectral sounder.
- Measurement precision is generally based on radiation temperature in the unit of K. If quantitation precision (bit) or signal-noise ratio (S/N) is required, a value and the unit are stated in each case.
- Figures in braces in the Precision or Application field present appropriate ranges of precision.
- Some fields are filled with a bar because of "Not applicable," "To be determined because of contemplation" or "Insufficient information."
- Abbreviations in the Wavelength & Frequency field represent the following: V: Vertical; H: Horizontal; L: Left; R: Right; +45: +45 degree polarization; and -45: -45 degree polarization. To show only the number (n) of polarization states, add "Pn" before a figure. None of these symbols in a field shows that polarization is not classified.
- To show the number of bands, add [B] before a number.
- To show vertical resolution, add [V] before a number.

Name of satellite series or program	Satellite name	Sensor name	Sensor type	Wavelength [μm] Frequency [GHz]	Number of channels	Measurement precision [K]	Spatial resolution [km]	Application	Launch date (other information)
GeoStationary Satellite									
MTSAT Japan	MTSAT-1R	JAMI	IR_VIS-I	[VIS] 0.55-0.90 [IR] 10.3-11.3 11.5-12.5 6.5-7.0 3.5-4.0[μm]	5	[VIS] 6.5 (2.5% albedo) [IR1] 0.18 [IR2] 0.18 [IR3] 0.15 [IR4] 0.18 (300K)	[VIS] 1 [IR] 4	Cloud distribution/ wind	Feb. 2005
	MTSAT 2	IMAGER	IR_VIS-I	[VIS] 0.55-0.90 [IR] 10.3-11.3 11.5-12.5 6.5-7.0 3.5-4.0[μm]	5	[VIS] 6.5 (2.5% albedo) [IR1] 0.09 [IR2] 0.12 [IR3] 0.11 [IR4] 0.20 (300K)	[VIS] 1 [IR] 4	Cloud distribution/ wind	Feb. 2006

Name of satellite series or program	Satellite name	Sensor name	Sensor type	Wavelength [μm] Frequency [GHz]	Number of channels	Measurement precision [K]	Spatial resolution [km]	Application	Launch date (other information)
Polar Orbiting Satellite, and others									
CloudSat U.S. (NASA) Canada (CSA)	CloudSat	CPR	Cloud radar	94[GHz]	1	Calibration precision 1.5[dB]	2, [V]0.5	Three-dimensional distribution of clouds	Apr. 2006
DMSP U.S. (air force)	DMSP F13 14 15	SSM/I	MW-I	19.35VH 22.24V 37.0VH 85.5VH[GHz]	7	0.6	69×43	Atmospheric temperature, water vapor (vertical) distribution, precipitable water, precipitation intensity [mm/hr], ocean surface wind speed [m/s]	Mar. 1995 Apr. 1997 Dec. 1999
						0.6	60×40		
						0.6	37×28		
						1.1	15×13		
		SSM/T1	MW-S	50.5 -59.4[GHz]	7	-	Diameter 174		
						SSM/T-2	MW-S	91.5, 150,183[GHz]	5
	F16	SSMIS	MW-IS	19.35VH 22.235V 37VH 91.655VH 60,63 50.3-59.4H 150H 183H[GHz]	24				
	17					0.45	46.5×73.6	Sea surface temperature [2K], sea-ice distribution, ice concentration, snow cover, and solid moisture distribution	Nov. 2006
	18					0.22	31.2×45.0		Oct. 2007
	19					0.19	13.2×15.5		Apr. 2009
	20					0.38-1.23	75.2×75.0-37.7-38.8		Oct. 2011
						0.20-0.26	37.7×38.8		
						0.53	13.3×15.5		
	0.38-0.56					13.2×15.5			

Name of satellite series or program	Satellite name	Sensor name	Sensor type	Wavelength [ $\mu\text{m}$ ] Frequency [GHz]	Number of channels	Measurement precision [K]	Spatial resolution [km]	Application	Launch date (other information)		
EOS U.S. (NASA)	Aqua	MODIS	IR_VIS-I	0.4-14.4 [ $\mu\text{m}$ ]	36	0.05(300K)	0.25, 0.5, 1	Clouds, ground information, SST, sea-ice ratio, wind	May 2002		
		AMSR-E	MW-I	6.925 VH, 10.65 VH, 18.7 VH, 23.8 VH, 36.5 VH, 89.0 VH [GHz]	12	0.3 0.6 0.6 0.6 1.1	74 $\times$ 43 51 $\times$ 30 27 $\times$ 16 32 $\times$ 18 14 $\times$ 8 6 $\times$ 4	Precipitable water, sea surface wind speed, sea surface temperature, sea-ice distribution and soil moisture distribution			
		AMSU-A	MW-S	Same as NOAA							
		HSB	MW-S	150,183[GHz]	4	-	13.5km	Vertical distribution of amount of water vapor			
		AIRS	IR-HS	649-1135, 1217-1613, 2169-2674[1/cm]	2378	0.15-0.35	13.5	Atmospheric temperature, vertical distribution of amount of water vapor, land/sea surface temperature, cloud characteristics, and radiation energy flux			
		CERES	Net radiometer	0.3-5, 8-12, 0.3-50 [ $\mu\text{m}$ ]	3	Shortwave radiation 2% Longwave radiation 1%	21km	Radiation balance			
	Terra	MODIS	IR_VIS-I	Same as Aqua							Dec. 1999
		ASTER	VIS_IR-I	0.5-0.9	3	8[bit]	15m	Clouds, land usage, sea surface temperature			
				1.6-2.5	6	8[bit]	20m				
				8-12 [ $\mu\text{m}$ ]	5	0.3, 12[bit]	90m				
		MISR	Multidirectional radiometer	0.45,0.56, 0.57,0.87 [ $\mu\text{m}$ ]	4	-	0.24,0.48, 0.96,1.92	Albedo, aerosol			
	MOPITT	Tropospheric contamination monitor	2.2-4.7 [ $\mu\text{m}$ ]	8	-	22 $\times$ 22	Tropospheric contamination monitoring				
	CERES	Net radiometer	Same as Aqua								
	Aura	OMI	Atmospheric chemical sensor	0.350-0.5, 0.270-0.314, 0.306-0.38 [ $\mu\text{m}$ ]	-	Spectral resolution 1.0-0.45 [ $\mu\text{m}$ ]	13 $\times$ 25	Ozone distribution [1-5%]	Jul. 2004		
		TES	Tropospheric radiometric spectrometer	2.3-15.4 [ $\mu\text{m}$ ]	-	Spectral resolution 0.025-0.1 [1/cm]	0.53 $\times$ 5.3	Chemical distribution			
		HIRDLS	Sounder for peripheral observation	6.12-17.76 [ $\mu\text{m}$ ]	21	-	500, [V]	Chemical distribution			
		MLS	MW rim sounder	118, 190, 240, 640, 2500[GHz]	5	Spectral resolution 5[MHz]	5 $\times$ 500	Amount of water vapor in upper convection sphere			

Name of satellite series or program	Satellite name	Sensor name	Sensor type	Wavelength [μm] Frequency [GHz]	Number of channels	Measurement precision [K]	Spatial resolution [km]	Application	Launch date (other information)
GCOM-W Japan (JAXA)	GCOM-W1 -W2 -W3	AMSR2	MW-I	6.925VH 7.3VH 10.65VH 18.7VH 23.8VH 36.5VH 89.0VH [GHz]	14	0.34 0.7 0.7 0.6 0.7 1.2	35×62 24×42 14×22 15×26 7×12 3×5	Precipitable water, precipitation intensity, sea surface wind speed, sea surface temperature, sea-ice distribution, ice concentration, snow cover, and soil moisture distribution	Three satellites are planned to be launched every four years starting around 2011-2012
GCOM-C Japan (JAXA)	GCOM-C1 -C2 -C3	SGLI	IR_VIS-I	[VN]380-565 670P3, 865P3 [nm] [SW]1050-2210 [nm] [T]10.8,12.0 [μm]	[B] 19	12[bit]	[VN] 0.25-1 [P] 1 [SW] 0.25-1 [T] 0.5	Observation of atmospheric and ground conditions relevant to carbon cycle and radiation balance	Three satellites are planned to be launched every four years starting around 2012-2013
GOSAT Japan	GOSAT	TANSO-FTS	Infrared spectrometer	0.76,1.6, 2.0,6-15[μm]	[B]4	Spectral resolution 0.2[1/cm]	10.5	Carbon dioxide level (1%)(4 ppmv)	Aug. 2008
		TANSO-CAI	IR_VIS-I	0.38,0.67, 0.87,1.62[μm]	4	Spectral resolution 20-90[nm]	0.5-1.5	Cloud and aerosol distributions	
GPM Japan and U.S.	Main GPM satellite	DPR	2-Frequency precipitation radar	13.6,35.5[GHz]	2	-	-	Precipitation	2013 [observation system consisting of one main satellite and eight sub-satellites]
		GMI	MW-I	10.7,19.3,21,37, 89,165, 183[GHz]	-	-	-	Cloud and precipitation characteristics	

Name of satellite series or program	Satellite name	Sensor name	Sensor type	Wavelength [μm] Frequency [GHz]	Number of channels	Measurement precision [K]	Spatial resolution [km]	Application	Launch date (other information)
NOAA U.S. (NOAA)	NOAA15 16 17	HIRS/3	IR-S	069, 3.76-4.57, 6.72-14.95[μm]	20	13[bit]	20.4	Vertical distributions of atmospheric temperature and amount of water vapor	May 1998 Sep. 2000 Jun. 2002
		AMSU-A	MW-S	23.8, 31.4, 89.0, 50.3-57.3[GHz]	15	0.25-1.20	48	Vertical distribution of atmospheric temperature	
		AMSU-B	MW-S	89.0, 150.3 183 [GHz]	5	0.37-1.06	16	Vertical distribution of amount of water vapor	
		AVHRR/3	IR_VIS-I	[VIS] 0.58-0.68 [IR] 0.725- 1.1,1.6, 3.55-3.93, 10.3-11.3, 11.4-12.4[μm]	6	10[bit] 0.12	1.1	Cloud distribution, discrimination between snow and ice, and sea surface temperature	(Note: SBUV/2 will be loaded onto successor satellites to NOAA16)
		SBUV/2	Atmospheric chemical sensor	0.252-0.34 [μm]	12	14[bit]	170	Vertical distribution of ozone [1-5%]	
	NOAA18	HIRS/4	IR-S	069, 3.76-4.57, 6.72-14.95[μm]	20	13[bit]	10.2	Same as HIRS/3	May 2005
	NOAA N'	MHS	MW-S	89.0,157, 183, 190[GHz]	5	0.22-0.51	16	Same as AMSU-B	Dec. 2008
	AMSU-A SBUV/2 AVHRR/3	See information about NOAA15-17							



Name of satellite series or program	Satellite name	Sensor name	Sensor type	Wavelength [μm] Frequency [GHz]	Number of channels	Measurement precision [K]	Spatial resolution [km]	Application	Launch date (other information)
QuikSCAT U.S. (NASA)	QuikSCAT	SeaWinds	MW Wave scattering monitor	13.4[GHz]	1	-	25	Sea surface wind ( RMSE 2[m/s]{3- 20m/s} 20[deg])	Jun. 1996
TRMM Japan (NASDA) U.S. (NASA)	TRMM	TMI	MW-I	10.7VH, 19.35VH, 21.3V, 37.0VH, 85.5VH [GHz]	9	VH 0.63/0.54 0.50/0.47 0.71 0.36/0.31 0.52/0.93	73×42 35×21 31×21 18×11 8×5	Precipitable water, sea surface wind speed, sea surface temperature, sea-ice distribution, and soil moisture distribution	Nov. 1997
		PR	Precipitation radar	13.796, 13.802 [GHz]	-	-	4.3 [V] 0.25	Three- dimensional precipitation distribution (0.7 mm/hr)	
		VIRS	IR_VIS-I	0.63, 1.6, 3.75, 10.8, 12.0 [μm]	5	-	2	Cloud distribution, and estimation of precipitation	
		CERES	Net radiometer	0.3-5, 8-12, 0.3-50[μm]	3	Shortwave radiation 2% Longwave radiation 1%	21km	Radiation balance	

Reference URLs

<http://www.restec.or.jp/databook/>  
<http://www.data.kishou.go.jp/satellite/satellite.html>  
<http://www.ipo.noaa.gov/lams/index.html>  
<http://www.esa.int/esaCP/index.html>  
<http://www.nasa.gov/>